DISTRIBUTION STATEMENT A

Approved for public release;
Distribution Unlimited

DTIC QUALITY INSPECTED &

19960819 100

Dynamical Systems

t=0

t=1/24
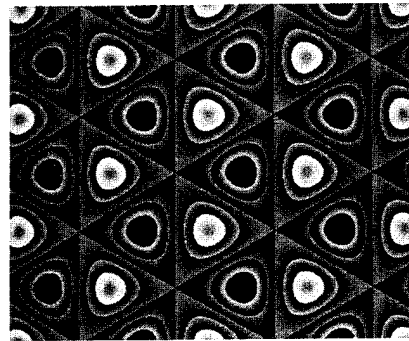
t=1/12
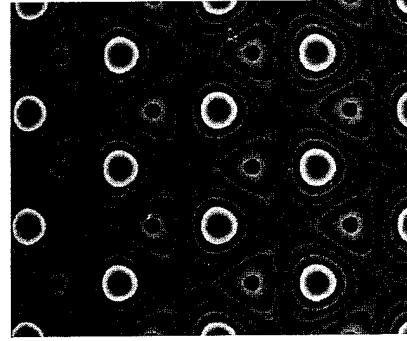
t=1/8
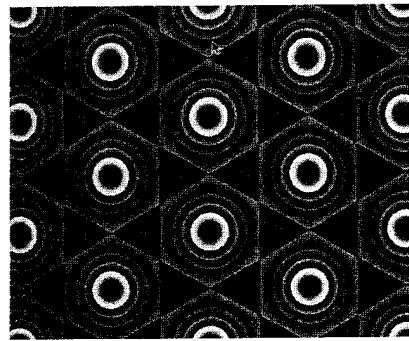
t=1/6

Oscillating Triangles

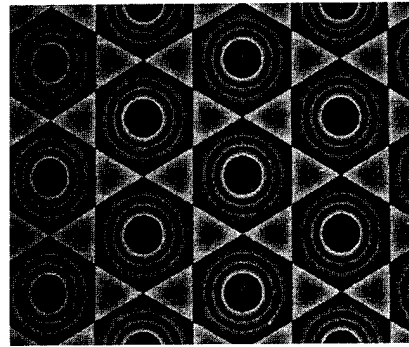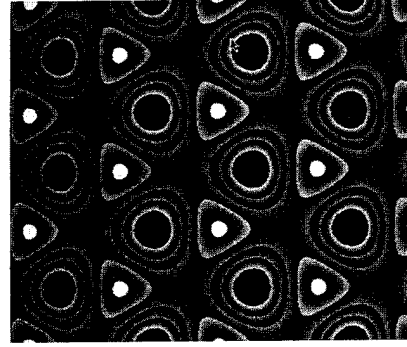These figures show one of the several remarkably stable and robust structures of the equations that model double diffusion convection. In such flows, thermal effects and density stratification (salinity) compete to form complex equilibrium structures. The snapshots in this figure show the cross section of the state of a periodic solution known as "oscillating triangles", where the structure is neither a standing wave nor a traveling one. For more details of the possible patterns in the double diffusion equations, see the article by Y. Renardy in this issue.

Articles

Departments

About the Cover

The three pictures on the cover show the perturbation of a fluid flow with the so-called cusped jet velocity profiles. Such velocity fields commonly arise in the analytical modeling of oceanic jets, such as the Gulf Stream. The main issue is to understand the mechanism for the transport of fluid particles across such oceanic jets. The top figure shows the effect of adding a secondary wave to the model of meandering jet whose unperturbed shape consisted of a string of cat's eyes. The middle figure shows the dynamics of a velocity profile for a double cusped jet prior to perturbation. The bottom figure shows the break-up of the neteroclinic and homoclinic tangles in this flow when a secondary neutral mode is added to the model. More details about these figures can be found in the article by Jones et. al. in this issue.

Dynamical Systems and Ocean Dynamics

Reza Malek-Madani, Guest Editor
Office of Naval Research

Introduction

Since the seminal works of Liapunov and Poincaré, research in dynamical systems has provided scientists with a set of practical tools to investigate the qualitative behavior of solutions of differential equations. In the past fifty years this area of mathematics has produced some of the most insightful and precise information about the nature of the dynamics present in many important applications ranging from biology to physics. Recently, a group of applied mathematicians joined together in a concerted effort to develop dynamical systems tools appropriate for problems in ocean dynamics. The articles that follow will give an introduction to these methods and provide a sample of the type of questions that one can properly pose and answer in a dynamical system setting, and point to the future directions of research.

The mathematical modeling of the ocean is a relatively young science that still takes many of its cues from observation and experimentation. Although the basic governing equations have been well-known for many decades, a large class of partial differential equations are present in the literature whose derivations depend on the special scales in the geometry of the region of interest as well as the strength of the forces involved. In addition to the information one draws from these models, a substantial amount of data is collected, either remotely or in-situ, that has contributed significantly to our understanding of the basic phenomena as well as challenged some of the underlying assumptions that have led to the mathematical models. One approach to reducing the gap between the sophis-tication and physical realism of the mathematical models and the information gathered in real data is to develop mathematical tools that are not so heavily model dependent that they lose their significance when one mathematical model is discarded in favor of another. With this point in mind, the methods and techniques outlined in the next three articles in this journal aim at understanding the basic issues that describe transport and mixing in the ocean and atmosphere as well as quantifying the competition among the forces that lead to double diffusion convection.

Computational models have been traditionally the widely used tool for predicting the response of the ocean and the atmosphere to various mechanical and thermodynamical proc-esses. In many respects, these efforts have closely followed the development of the numerical analysis of the Navier-Stokes equation and have attempted to find the appropriate range of various viscosity parameters that would lead to rea-sonable numerical simulations. This strategy has paid off well in the context of low Reynolds number dynamics mod-eled by this equation while it is a rich area of research for high Reynolds number turbulence. Because the Navier-Stokes equations are generally considered the correct mathematical model for many applications, it is felt that the investment of resources in developing more accurate numerical schemes for this specific equation is worthwhile. (See reference 1 for a viable alternative to a direct discretization of the Navier-Stokes equations, whether using finite difference methods, finite elements, or the various quasi-spectral methods that are currently being used in the literature). It is not clear that this

strategy is correct, or even desirable in ocean dynamics, considering the fact that more than one candidate for the "standard" model exists. It then seems reasonable that the solutions of the governing differential equations are understood at a level beyond the usual listing and tabulating the various values of the parameters and instead search for the coherent structures that are commonly present in these models.

This is not to diminish the role of numerical analysis in ocean dynamics. In fact, quite the opposite result is anticipated. The intent of the new dynamical systems methodology is to elucidate the common complex structures in the set of relevant systems of partial differential equations. Once the coarse properties of these structures are identified, numerical simulations on a reasonably small and computationally tractable number of initial conditions will reveal the finer properties of the mathematical models.

Scope of Applications

The mathematics described in the following articles is divided in two categories, depending on whether the models have a Lagrangian formulation or an Eulerian one. In the articles of S. Wiggins[2] and C. Jones et. al.[3] of this issue, the goal is to understand the nature of the solutions of the perturbed systems of ordinary differential equations that arise in the Lagrangian setting of motions in the ocean and atmosphere. This point of view is specially significant in ocean dynamics in light of the type of data taken from the so-called Lagrangian drifters that provide real data about various fluid particles in the ocean. Because only a finite (and a relatively small) number of these drifters are available at the present time, one is left with the challenging task of gathering information about a portion of the ocean from a handful of particle trajectories. This fact alone shows the acute need for a kind of mathematical analysis that goes well beyond the tabulation of parameter values.

The methods that are discussed in references 2 and 3 show how certain structures associated with invariant regions of an unperturbed dynamical system are transported by the perturbed velocity fields. Specific and delicate mathematical tools are developed to monitor the transport of information for a rather large class of perturbations. One of the intriguing problems that will be addressed in the future by these investigators is what happens to these dynamical systems methods when, as is the case in real life, the velocity fields that the differential equations are based on are only known on a *discrete* set of points in the ocean. A related problem is whether one can develop systematic mathematical tools that can distinguish the effect of chaos from stochasticity in data sets that exhibit complex and coherent structures.

The article by Y. Renardy of this issue[4] addresses the set of partial differential equations that model double diffusion convection. This paper shows how to use the center manifold theorem of dynamical systems and classify the stability properties of certain important solutions of the original system. A central feature of this theorem is in its ability to reduce the analysis of the dynamics to a lower order system. Various traveling wave solutions of the original governing system of partial differential equations are identified and numerically simulated.

References

1. A. Eden, C. Foias, B. Nicolaenko and R. Temam, *Exponential Attractors for Dissipative Evolution Equations*, Masson, Paris, J. Wiley, Boston, 1994.

2. S. Wiggins, *Lagrangian Transport in Geophysical Flows: New Approaches and Techniques from Dynamical Systems*, Naval Research Review, this issue.

3. C. K. R. T. Jones, G. Haller, P.D. Miller, J. Rubin, *Settling and Chaotic Mixing in Oceanic Flows: the Role of Heteroclinic Orbits*, Naval Research Review, this issue.

4. Y. Renardy, *Planforms at the Onset of Instability in Double Diffusion Convection*, Naval Research Reviews, this issue.

Lagrangian Transport in Geophysical Flows: New Approaches and Techniques from Dynamical Systems Theory

Stephen Wiggins
Applied Mechanics, and Control and Dynamical Systems
California Institute of Technology

Introduction

The *standard map* is a two-dimensional area-preserving transformation, or *dynamical system*, that has been the subject of literally hundreds of papers in the dynamical systems community over the past twenty years. The map is given as follows

$$x \to x+y-\pi,$$

$$y \to y+k\sin(x+y),$$

and it is periodic in x and y. In Figure 1 we plot a single orbit of this map for different initial conditions in each of the four panels for the parameter value $k=1$. (By the term "orbit" we mean a sequence of points obtained by iterating a given initial point according to the map. Thus an orbit of a map is a discrete time trajectory.) The orbits in the upper left hand and lower right hand panels explore a significant fraction of the phase space. Moreover, the motion is chaotic in the sense that nearby orbits separate at an exponential rate. However, note the "holes" in the regions. The chaotic regions do not fill all of the space. Note the difference in the orbits in the upper right hand and lower left hand panels. These orbits appear to lie on closed curves. There are four discrete closed curves in the former case and one closed curve in the latter case. Orbits on these curves

separate at a linear rate. These closed curves are examples of "KAM tori" and are boundaries which orbits cannot cross. KAM tori are examples of lower dimensional "phase space structures" that evidently have a marked influence on transport in phase space.

The chaotic regions are built on the skeleton of a lower dimensional phase space structure. In Figure 2 we show some intertwining one dimensional curves that lie in the chaotic region in the upper left hand panel of Figure 1. These curves are the one dimensional *stable and unstable manifolds* of the saddle type fixed point in that region. They are the mechanism giving rise to the chaos, and they also govern the transport through such chaotic regions and play a very important role in understanding this phenomena.

Thus, in this example we see that the phase space is a mixture of "regular" and chaotic regions, a situation that we now know is typical for many nonlinear dynamical systems. Moreover, lower dimensional "phase space structures"–KAM tori, stable and unstable manifolds of periodic orbits–form the skeleton in phase space upon which the regions of regular and chaotic motions exist.

Despite the simplicity of this example, the same mathematical framework and ideas have implications and uses for many problems in geophysical fluid dynamics, and we next

want to motivate this setting and approach. Suppose one is interested in the motion of a *passive tracer* in a fluid (e. g. dye, temperature, or any material that can be considered as having negligible effect on the flow), then, *neglecting molecular diffusion*, the passive tracer follows fluid particle trajectories which are solutions of

$$\dot{x} = \upsilon(x,t;\mu), \tag{1}$$

where $\upsilon(x,t;\mu)$ is the velocity field of the fluid flow, $x \in IR^n$, $n = 2$ or 3, and $\mu \in IR^p$ represent possible parameters. When viewed from the point of view of dynamical systems theory, the phase space of (1) is actually the physical space in which the fluid flow takes place. Evidently, "structures" in the phase space of (1) should have some influence on the transport and mixing properties of the fluid. To make this more precise, let us consider a fluid mechanically more simplified situation that can be related directly to the standard map example described above. Suppose that the fluid is two-dimensional, incompressible, and inviscid, then we know that the velocity field can be obtained from the derivatives of a scalar valued function, $\psi(x_1,x_2,t;\mu)$, known as the *stream function*, as follows

$$\dot{x}_1 = \frac{\partial \psi}{\partial x_2}(x_1,x_2,t;\mu),$$

$$\dot{x}_2 = -\frac{\partial \psi}{\partial x_1}(x_1,x_2,t;\mu), \qquad (x_1,x_2) \in IR^2. \tag{2}$$

Figure 1.

Four orbits of the standard map for k=1.
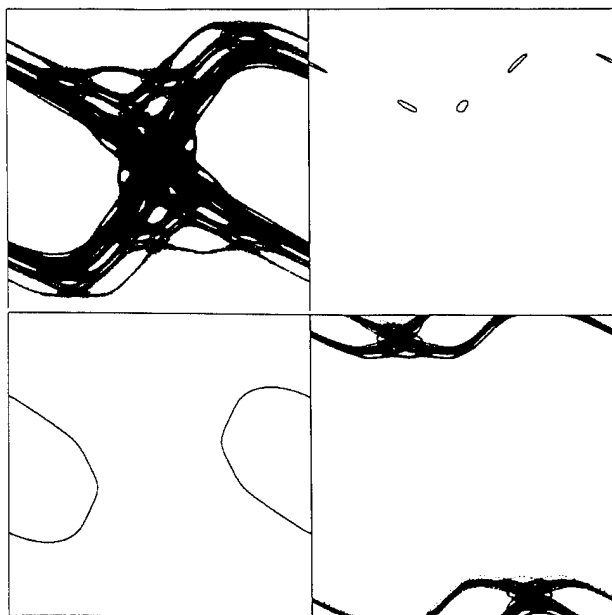
In the context of dynamical systems theory, (2) is a time-dependent Hamiltonian vector field where the stream function plays the role of the Hamiltonian function. If the flow is time-periodic then the study of (2) is typically reduced to the study of a two-dimensional area preserving *Poincaré map*, of which the standard map is an example. Practically speaking, the reduction to a Poincaré map means that rather than viewing a particle trajectory as a curve in continuous time, one views the trajectory only at discrete intervals of time, where the interval of time is the period of the velocity field. The value of making this analogy with Hamiltonian dynamical systems lies in the fact that a variety of techniques in this area have immediate applications to, and implications for, transport and mixing processes in fluid mechanics. For example, the persistence of invariant curves in the Poincaré map (KAM curves) gives rise to barriers to transport, chaos and Smale horseshoes provide mechanisms for the "randomization" of fluid particle trajectories, an analytical technique, Melnikov's method, allows one to estimate fluxes as well as describe the parameter regimes where chaotic fluid particle motions occur, a relatively new technique, lobe dynamics, enables one to efficiently compute transport between qualitatively different flow regimes, bifurcation theory enables one to understand how qualitatively different flow regimes appear and disappear as system parameters are varied, etc. In short, many new methods for the study of fluid transport and mixing are available from dynamical systems theory. In the following we will show how this framework and techniques can be used in a problem of geophysical interest.

The techniques and results described in the following have been obtained over the past few years in collaboration with my colleagues Anthony Leonard and John Brady at Caltech, and former graduate students Vered Rom-Kedar, Roberto Camassa, Tasso Kaper, Darin Beigie, and Igor Mezic′.

Transport in a Cellular Flow: The Physical Setting and the Model Flow

The physical setting that we consider is as follows. We consider a (steady) convection cell whose horizontal length is much larger than its height and where the convection cells are aligned along the y-axis (Figure 3). In this situation the flow is essentially two-dimensional and, assuming stress-free boundary conditions and single-mode convection, an explicit form of the velocity field is given by (see Chandrasekhar [1961])

$$\dot{x} = -\frac{A\pi}{k} \cos(\pi z) \sin(kx) = -\frac{\partial \psi}{\partial z}(x,z), \tag{3}$$

$$\dot{z} = A\sin(\pi z)\cos(kx) = \frac{\partial \psi}{\partial x}(x,z), \tag{4}$$

where

$$\psi(x,z) = \frac{A}{k} \sin(kx) \sin(\pi z),$$

A is the maximum vertical velocity in the flow,

$$k = \frac{2\pi}{\lambda}$$

(λ the wavelength associated with the cell pattern), and the length measures have been non-dimensionalized so that the top is $z=1$ and the bottom $z=0$. This flow has a countable infinity of saddle type stagnation points, or *hyperbolic fixed points* in dynamical systems terminology, on the upper boundary at

$$(x,z) = (\frac{j\pi}{k},1), j = 0,\pm1,\pm2,...$$

and a countable infinity of hyperbolic fixed points on the lower boundary at $(x,z) = (\frac{j\pi}{k},0), j = 0,\pm1,\pm2,....$ Fixed points with the same x coordinate are connected by a stagnation streamline, or *heteroclinic orbit* in dynamical systems terminology. The result is an infinite number of cells, and many of the fluid mechanical problems of interest are concerned with the transport of a passive tracer from cell-to-cell. Fluid flows which are divided up into a collection of cells occur in a variety of geophysical

Figure 2.

Stable and unstable manifolds of a period one point in a chaotic region.
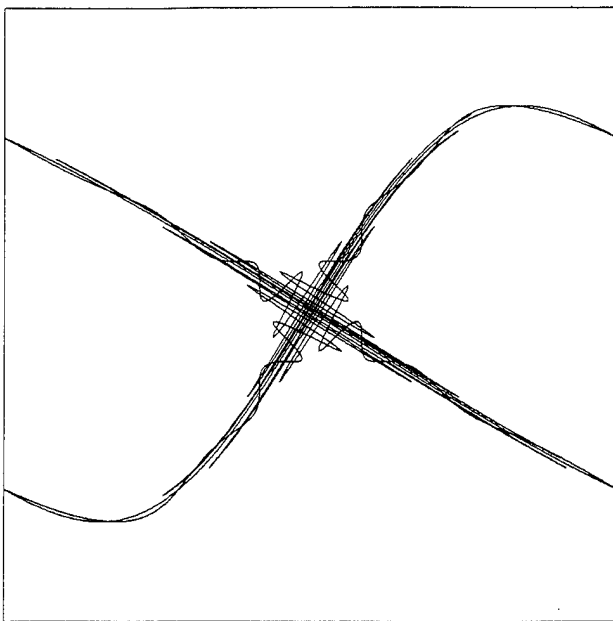
applications and the methods and approaches discussed in this article in principle can be applied to any such *cellular flow*.

The Experiments of Solomon and Gollub

We motivate the analysis by discussing some experiments of Solomon and Gollub on this system. If the temperature difference between the top and bottom of the convection cell is increased an additional time-periodic instability occurs, resulting in a time-periodic velocity field (Clever and Busse [1974], Bolton et al. [1986]). Solomon and Gollub [1988] experimentally studied the transport of dye in such a flow and they made the following observations.

1. There was a dramatic enhancement of the "effective diffusivity".

2. Molecular diffusion appeared to play no role in the transport.

3. The flux across the cell boundaries (heteroclinic orbits) depended linearly on the amplitude of the oscillatory instability and was independent of the wavelength λ.

Therefore, the transport problem is radically different in the unsteady case as compared to the steady case since in the steady case streamlines cannot cross and therefore tracer crosses the cell boundaries solely as a result of molecular diffusion. In order to study these issues Solomon and Gollub introduced the following model of the *even oscillatory cell instability*:

$$\dot{x} = -\frac{A\pi}{k}\cos(\pi z)[\sin(kx) + \varepsilon kf(t)\cos kx)] = -\frac{\partial\psi}{\partial z}(x,z,t)$$

$$\dot{z} = A\sin(\pi z)[\cos(kx) - \varepsilon kf(t)\sin(kx)] = \frac{\partial\psi}{\partial x}(x,z,t) \qquad (5)$$

where

$$\psi(x,z,t) = \frac{A}{k}\sin(kx)\sin(\pi z) + \varepsilon f(t)\cos(kx)\sin(\pi z)$$

and we will take

$$f(t) = \cos(\omega t) \text{ and } \varepsilon \sim (R - R_c)^{1/2},$$

where R is the Rayleigh number and R_c its critical value at which the time-periodic instability occurs. The pros and cons of this model are discussed in Solomon and Gollub [1988]. This model will be the starting point of our analysis and, motivated by the experimental observations of Solomon and Gollub, we will consider the following four questions.

1. What is the mechanism for cell-to-cell transport?

2. Can we quantify the spreading of a passive tracer (dye) initially contained in one cell?

Figure 3.

Streamlines for the steady, cellular flow.
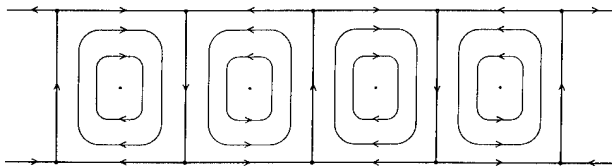
3. Can we predict the number of cells invaded as a function of time?

4. What are the effects of the addition of a small amount of molecular diffusion?

The Mechanism for Cell-to-Cell Transport

In the case of unsteady two-dimensional flows modern dynamical systems theory provides us with some new methods and concepts that enable us to analyze the particle kinematics. For example, the saddle-type stagnation points may move and the separatrices associated with different "moving stagnation points" typically will not coincide to form cell boundaries in the flow. This situation can lead to cell-to-cell transport. Very roughly speaking, dynamical systems theory provides us with methods for studying particle kinematics in unsteady flows with moving stagnation points and their associated moving separatrices. For the case of time-periodic variability, if the variability is weak then it can be shown that a saddle-type

stagnation point persists, but it oscillates periodically in time (with the period of the variability). Moreover, this "oscillating stagnation point" (more precisely, *hyperbolic periodic orbit*) still maintains its saddle-type stability characteristic and associated with it are two one-dimensional periodically varying curves called the *stable and unstable manifolds of the hyperbolic periodic orbit*. Trajectories on the stable manifold approach the hyperbolic periodic orbit asymptotically as $t \to \infty$ and trajectories on the unstable manifold approach the hyperbolic periodic orbit asymptotically as $t \to -\infty$. These curves are invariant curves in the sense that particle trajectories that start on the curves remain on the curves *for all time*. This property of invariance implies that other trajectories cannot cross these curves, hence they act as barriers to fluid transport in a way that we will describe more fully shortly. These curves are the unsteady analogs of the separatrices that commonly arise in steady flows. However, as opposed to the steady case, the stable and unstable manifolds of different oscillating saddle-type stagnation points typically do not coincide to form complete barriers to fluid transport. Rather, at a fixed instant of time they may intersect in a discrete set of points. Nevertheless, these curves still have the important kinematical effect of forming the boundaries between fluid particle trajectories that move in different directions after their encounter with the oscillating saddle-type stagnation point. However, since the stable and unstable manifolds of different oscillating saddle-type stagnation points need not join up (and, hence, form a curve of finite length in the flow), they may have infinitely long length and wind throughout the flow (and themselves) in a complicated geometrical fashion. Keeping in mind the kinematical meaning of these curves as boundaries between qualitatively different fluid particle motions, they therefore act as *partial barriers* to fluid transport. As a result, fluid transport in two-dimensional unsteady flows may be much more varied and complex. Dynamical systems theory gives us a way to make these intuitive notions precise and quantitative, which we now describe for time-periodic variability.

For time-periodic variability a variety of standard dynamical systems techniques and results make it advantageous to consider particle kinematics via the so called *Poincaré map*, which we will denote by *f*. That is, rather than plotting a particle trajectory as a continuous curve in space one plots its evolution at discrete intervals of time, where the interval of time is equal to the period of the variability. In this setting, the oscillating saddle-type stagnation point is manifested as a *fixed point* of the Poincaré map and the stable and unstable manifolds associated with the fixed point are similarly fixed in space for the Poincaré map. Consequently, the situation bears some similarity to the steady case, but it is important to keep in mind that for the Poincaré map particle trajectories are manifested as sequences of discrete points, rather than continuous curves. Also, as we mentioned earlier, the stable and unstable manifolds of different hyperbolic fixed points may

Figure 4.

The behavior of the stable and unstable manifolds on the walls of the convection cell under the time-periodic perturbation– the heteroclinic tangle, numerically calculated for $\varepsilon = 0.1$, $\omega = 0.6$, $A = 0.1$.
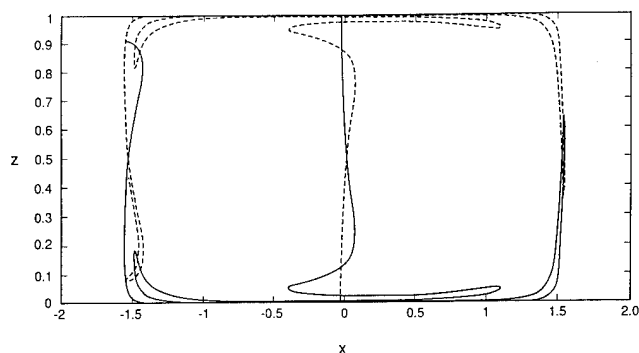
not coincide(or "join up") to make a separatrix of finite length, rather they may intersect in a discrete number of points and wind throughout the flow. We demonstrate this for (5) in Figure 4. The stable and unstable manifolds of the different hyperbolic fixed points actually have infinite length, but we obviously can only show a finite portion of each in the figure. Next we show how the geometric structure associated with the stable and unstable manifolds of the different hyperbolic fixed points influence transport.

For the Poincaré map, segments of finite length of the stable and unstable manifolds of the hyperbolic fixed points can be used to form cell boundaries. We illustrate this in Figure 5 where the segments of finite length begin at the hyperbolic fixed points and end at particular intersection points of the stable and unstable manifolds, which we will refer to as the *boundary intersection points*. Now we can consider the question of fluid exchange between the different regions defined by our chosen boundaries that are shown in Figure 5.

First we list two rules that points on the stable and unstable manifolds of hyperbolic fixed points must obey under iteration by the Poincaré map. (By "iteration" we mean repeated application of the Poincaré map to a particle or, in other words, discrete time evolution of a particle trajectory.)

1. A point that is on *both* the stable and unstable manifolds must remain on both manifolds under all positive and negative iterations of the Poincaré map. This is because these manifolds are *invariant manifolds*.

2. Points on the stable or unstable manifolds of a fixed point maintain their relative order (in the sense of distance in arc length from the fixed point) under iteration by the Poincaré map. That is, if we consider two distinct points on the stable or unstable manifold then one will be closer than the other to the fixed point in the sense of arc length along the stable or unstable manifold. If we

then iterate both points, the same point will always thereafter be closer to the fixed point. The reasons for this are more technical and are related to uniqueness of particle trajectories for a given initial condition.

With these two rules in mind let us return to Figure 5 and consider the preimages under the Poincaré map of the boundary intersection points, i. e. , the backwards time evolution of these points for one period of the variability. By rule 1 these points still lie on both the stable and unstable manifolds, and since the manifolds are smooth curves they must wind through each other as shown in Figure 6. In this figure we have shown also precisely one additional point of intersection of the manifolds between the boundary intersection point and its preimage. There is a technical reason for this that we briefly must mention. Generally, there must be an odd number of additional intersection points between the boundary intersection point and its preimage if we have uniqueness of parcel trajectories for a given initial condition. Without loss of generality, we can assume that we have one additional intersection point since all other cases can be recast in this form. Hence, the segments of the stable and unstable manifolds between a boundary intersection point and its preimage form two *lobes* and these two lobes are said to form a *turnstile*. The turnstiles are the mechanisms governing transport between the different regions, as we will now argue. Consider the image of the turnstile lobes under the Poincaré map f (i. e. , the evolution of these points for one period of the flow). Using the two rules above, as well as the fact that(for a continuous and continuously invertible map) the boundary of a set maps to the boundary of its image and the interior of a set maps to the interior of its image, we see that the image of the turnstile lobes appear as in Figure 6. Thus, the respective turnstile lobes have "switched sides" in relation to the boundary (hence the term "turnstile"). Now, using rule 2 above, it can be argued that the *only* points that cross the boundary in one iteration of the Poincaré map are those in the

Figure 5.

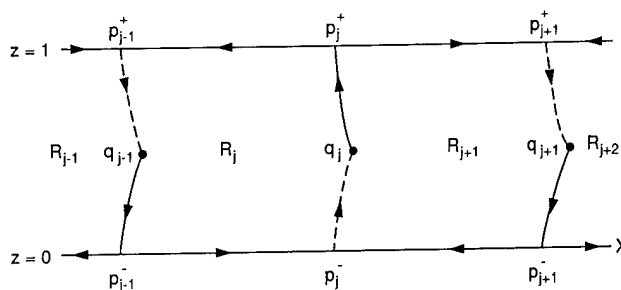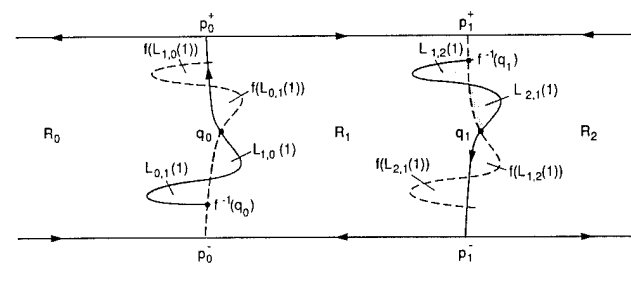*Cell boundaries for the unsteady flow(for the associated Poincaré map).*

Figure 6.

The turnstile lobes associated with cell-to-cell transport.

turnstile lobes. Therefore the *flux across the boundary in one period* is simply the area of the turnstile lobe.

In the case where the variability is weak there is a perturbation method that will enable us to estimate the lobe area–and therefore the flux per period–across the "broken separatrices". This is Melnikov's method for time-periodic vector fields. The Melnikov function is a measure of the distance between the stable and unstable manifolds measured along a line perpendicular to the unperturbed separatrix at the point parametrized by t_0, where t_0 can be thought of as an arc length parameter measuring distance along the unperturbed separatrix. In Camassa and Wiggins [1991] the Melnikov function on the zero phase cross section is calculated and found to be given by:

$$M(t_0) = \omega sech(\frac{\omega}{2A})\sin(\omega t_0),$$

Clearly the Melnikov function has a countable infinity of simple zeros, that correspond to a countable infinity of intersections of the stable and unstable manifolds.

As described above, the flux of fluid between cells is given by the area of the turnstile lobes. In this perturbative setting an approximation to the flux (lobe area) is given by the integral of the Melnikov function between two adjacent zeros, i. e.,

$$\mu(L_{1,0}(1)) = \mu(L_{0,1}(1)) = 2\varepsilon sech\frac{\omega}{2A} + \sigma(\varepsilon^2),$$

where μ ($L_{i,j}(1)$) denotes the area of the lobe $L_{i,j}$. We remark that because of translational symmetries, this result holds for all turnstile lobes. The symmetries of this problem are discussed in Camassa and Wiggins [1991]. This approximation to the flux show us that the flux depends linearly on the amplitude of the oscillatory instability and is independent of the wavelength of the cell patterns λ, exactly as observed experimentally by Solomon and Gollub.

The Number of Cells Invaded as a Function of Time: Lobe Dynamics

We next provide another example of how "lower dimensional structures" in the flow, the lobes, determine a large scale transport property of the flow. Suppose a given cell is filled with a passive tracer. How many cells are "invaded" by this tracer after some elapsed time? The answer to this question can be determined by the geometry of the lobe intersections associated with the cell boundaries. Using lobe dynamics type arguments and invariance of the manifolds, as well as translation and reflection symmetries, an upper and lower bound can be placed on the time that a passive scalar initially in R_1 first invades R_{-j}. Surprisingly, all the necessary information is contained in two integers which we refer to as the *signatures* of the heteroclinic tangles forming the cell boundaries, namely:

- $\bar{m}$ = the smallest integer such that $f^{\bar{m}}(L_{1,0}(1)) \cap L_{0,-1}(1) \neq 0$.
- $\bar{m}'$ = the smallest integer such that the boundary of $F^{\bar{m}'+\bar{m}}$ $(L_{1,0}(1))$ intersects the boundary of $L_{-1,-2}$ (1) in four distinct points

The signatures are illustrated in Figure 7 for $\bar{m} = 1$ and $\bar{m}' = 2$.

If we denote the period of the velocity field by $T = \frac{2\pi}{\omega}$ and t_j^{-j} the time necessary for tracer initially in R_1 to enter R_{-j} we have the following general result obtained in Camassa and Wiggins [1991]:

$$(\overline{jm} + 1)T \leq t_j^{-j} \leq [(j - 1)\bar{m}' + (\bar{m} + 1)]T, \ (j \geq 2).$$

Therefore, the upper and lower bounds for the first invasion time are completely determined by the signatures $\bar{m}$ and $\bar{m}'$. This result is independent of the boundary conditions. For instance,

Figure 7.

An illustration of the signatures of the heteroclinic tangle associated with the cell boundaries.
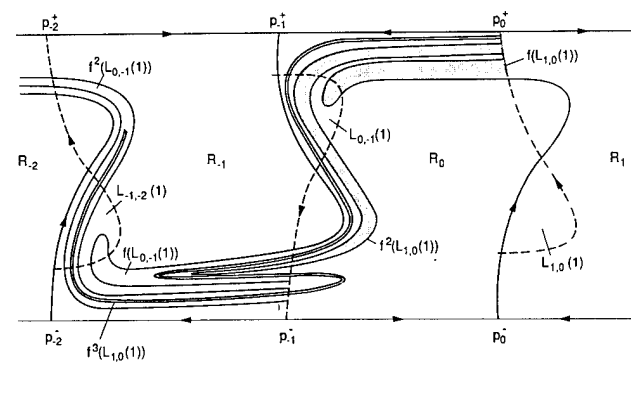
numerical computations show that in the case A=0. 1, ε = 0. 1 and ω =0.6 we have $\bar{m}$ and $\bar{m}'$=3 indicating that one cell is invaded every three periods, for A=0.1, ε = 0.1 and ω = 0.24 we have $\bar{m}$ and $\bar{m}'$ =1 indicating that one cell is invaded every period, and for A=0. 1, ε =0.01 and ω=0. 6 we have $\bar{m}$ and $\bar{m}'$ = 4 indicating that one cell is invaded every four periods. We remark that the signatures are very easy to compute numerically as one needs to compute only a(usually short) finite length of the manifolds. Moreover, the necessary manifold interections are typically robust with respect to numerical computations.

Quantifying the Spreading of a Passive Scalar: Lobe Dynamics

The dynamics of the turnstile lobes, *lobe dynamics*, can be used to rigorously determine the amount of tracer originally in one cell that is contained in any other cell at a later time. Suppose the cell R_1 is uniformly filled with tracer (species S_1) at t=0 how much of species S_1 is contained in R_j at any t > 0? If we denote by $T_{1,j}$ (n) the total amount of species S_1 in R_j immediately after the n-th iterate and by $a_{1,j}(n)$ =$T_{1,j}(n)$-$T_{1,j}(n-1)$ the flux of species S_1 into R_j on the n-th iterate , then it can be shown that this last formula can be reduced to an expression containing areas of intersection sets involving images of only one of the turnstile lobes $L_{1,0}(1)$ associated with the boundary of R_1. The resulting expression is given by

$$a_1 j(n) = T_1 j(n) - T_1 j(n-1) = (\delta_j 2 + \delta_j 0)\mu(L_{1,0}(1))$$

$$+ \sum_{k=1}^{n-1} \{2\mu\left(L_{j-1,j}(1)\cap f^k(L_{1,0}(1))\right) - 2\mu(L_{-j+2,-j}(1)\cap f^k(L_{1,0}(1)))$$

$$-2\mu\left(L_{j,j-1}(1)\cap f^k(L_{1,0}(1))\right) -2\mu\left(L_{j-1,j}(1)\cap f^k(L_{1,0}(1))\right)$$

$$+\mu\left(L_{j,j+1}(1)\cap f^k(L_{1,0}(1))\right) -\mu\left(L_{j,j+1}(1)\cap f^{k-1}(L_{1,0}(1))\right) \qquad (6)$$

$$-\mu\left(L_{j,j+1}(1)\cap f^k(L_{1,0}(1))\right) +\mu\left(L_{j,j+1}(1)\cap f^{k-1}(L_{1,0}(1))\right)$$

$$+\mu\left(L_{-j+2,-j+1}(1)\cap f^k(L_{1,0}(1))\right) -\mu\left(L_{j-2,k-1}(1)\cap f^k(L_{1,0}(1))\right)$$

$$-\mu\left(L_{j-2,j-1}(1)\cap f^{k-1}(L_{1,0}(1))\right) +\mu\left(L_{j-1,j-2}(1)\cap f^k(L_{1,0}(1))\right)\}$$

where, recall, μ ($L_{i,j}(1)$) denotes the area of the lobe $L_{i,j}(1)$. Consequently, a relatively straightforward numerical computation of $a_{1,j}(n)$ is possible. To compute $a_{1,j}(n)$ one merely locates the lobes indicated in (6), iterates $L_{1,0}(1)$ (i. e. , a grid of points covering $L_{1,0}(1)$), determines the area of intersection of the appropriate iterates of $L_{1,0}(1)$ with the other lobes in (6), and adds up the result according to the recipe provided by (6). Numerically this method is extremely efficient and affords tremendous savings in CPU time over standard "brute force" methods; details are discussed in Camassa and Wiggins

[1991]. However, practically, this computation can only be performed for a finite amount of time. In the next section we discuss an infinite time result.

Dispersion

Dispersion is a quantity that is frequently of interest in geophysical settings. For example, Pasmanter [1991] and Ridderinkhof and Zimmerman [1992] have recently studied dispersion in models of shallow tidal flows and found that it behaves asymptotically like t^2. Weiss and Knobloch [1989] have performed a numerical study of dispersion in modulated traveling waves in binary fluid convection and found a dispersion exponent of 1.93. As their results were numerical, they were only able to compute for a finite length of time. Using a

Figure 8.

Comparison of lobe dynamic transport results (solid) with transporttaking into effect molecular diffusivity (dashed) for the three cases. a) A= 0.1, ω = 0.6, ε = 0.1, b)A= 0.1, ω = 0.6, ε = 0.01.
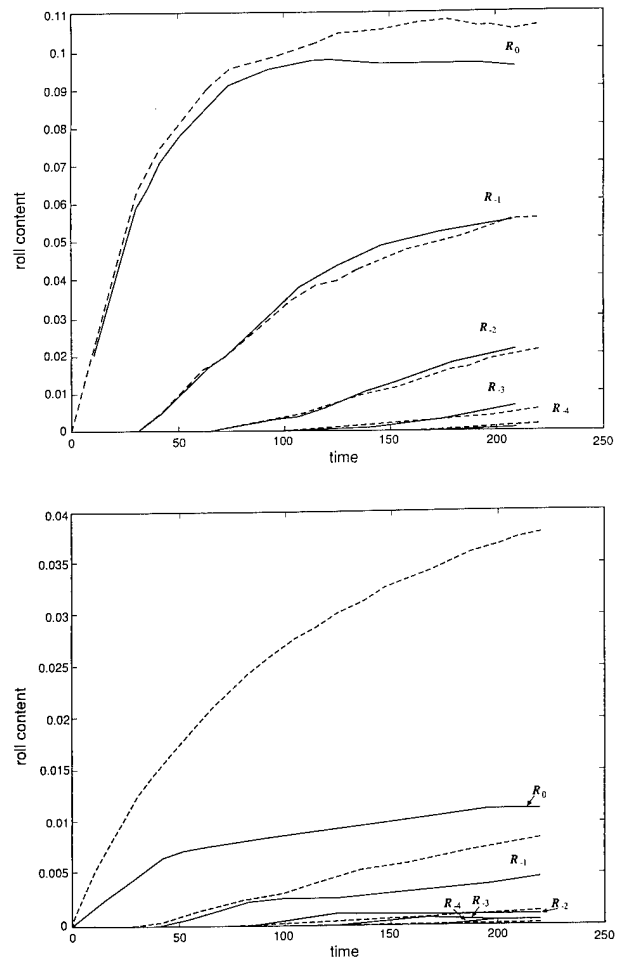
simple application of Birkhoff's ergodic theorem we can derive a rigorous result that applies in each of these settings and gives conditions under which the dispersion should behave asymptotically (in time) like t^2. As such, it may also prove to be a useful guide for numerical investigations. Our discussion will be in the context of the time-periodic cellular flow, however the results can be applied more generally(See Mezic' and Wiggins [1994b], [1994c]).

Referring to the velocity field (5), the displacement of a particle trajectory in the x direction is given by

$$x(t) - x(0) = \int_0^t \left(-\frac{A\pi}{k} \cos(\pi z(t)) [\sin(kx(t)) + \right.$$

(7)

$$\left. \varepsilon k \cos(\omega t) \cos(kx(t))] \right) dt,$$

where $(x(t), z(t))$ denotes a trajectory. For the application of Birkhoff's ergodic theorem we need to introduce a standard dynamical systems "trick" that is applied to time-periodic vector fields. That is, we introduce the phase, call it θ, of the time-periodic part as a new *dependent* variable and append it to the vector field. The new component is therefore $\dot{\theta} = \omega$ and the vector field is then viewed as a three-dimensional *time-independent* dynamical system. If D denotes the flow domain (periodic in x, bounded in z), then the phase space of this "enlarged" dynamical system is denoted $D \times S^1$, where S^1 denotes the phase of the time periodic part. The "flow" generated by this dynamical system is then denoted by $\Phi_t(x,z,\theta)$, i. e. , this is the trajectory that starts at the point (x, z, θ). If we denote the x component of the velocity of (5) by u, then (7) can be succinctly written as

$$x(t) - x(0) = \int_0^t u(\varphi_r(x,z,\theta)) dt, \qquad (8)$$

The mean square displacement or *dispersion* of the x component of (5) of an ensemble of points under the flow is given by

$$\langle (x(t) - x(0) - \langle x(t) - x(0) \rangle)^2 \rangle \equiv D_x(t),$$

where the average indicated by the angle brackets is defined as

$$\langle (x(t) - x(0) \rangle \equiv \int_{D \times S^1} (x(t) - x(0)) \, p d\mu,$$

$p = p(x, z, \theta)$ is the initial distribution of points (assumed to be bounded and integrable on $D \times S^1$), and $d\mu$ denotes the measure or "volume element" on $D \times S^1$. Incompressibility of the flow implies that the flow is "measure preserving", which is important for the application of Birkhoff's ergodic theorem.

We are interested in determining the asymptotic behavior of the dispersion. We have the following calculations:

$$\lim_{t \to \infty} \frac{D_x(t)}{t^2}$$

$$= \lim_{t \to \infty} \left\langle \left(\frac{1}{t} \int_0^t u \, (\varphi_\tau(x,z,\theta)) \, d\tau - \left\langle \frac{1}{t} \int_0^t u(\varphi_\tau(x,z,\theta)) d\tau \right\rangle \right)^2 \right\rangle,$$

$$= \left\langle \left(\lim_{t \to \infty} \frac{1}{t} \int_0^t u \, (\varphi_\tau(x,z,\theta)) d\tau - \left\langle \lim_{t \to \infty} \frac{1}{t} \int_0^t u(\varphi_\tau(x,z,\theta)) d\tau \right\rangle \right)^2 \right\rangle,$$

$$= \left\langle \left(u^*(x,z,\theta) - \dots u^*(x,z,\theta) \right) \right)^2 \right\rangle \equiv a.$$

1. The passage from the first to the second line is justified by the fact that the function u is bounded and integrable on $D \times S^1$. In the second line the limit

2. In the second line the limit

$$\lim_{t \to \infty} \frac{1}{t} \int_0^t U(\varphi_r(x,z,\theta)) dr \equiv u^*(x,z,\theta)$$

exists for all points in $D \times S^1$ by Birkhoff's ergodic theorem (see Arnold and Avez [1968]), *with the possible exception of a set of μ-measure zero*. This limit is the time average of the function w along the fluid particle trajectory that starts at the point (x, z, θ). Moreover, Birkhoff's ergodic theorem also guarantees that this limit is integrable. This, together with the boundedness of u, implies that the quantity a defined above is finite, and if it is nonzero, we can conclude that the dispersion of the ensemble of particles in the z direction behaves asymptotically like t^2.

Figure 9.

Contours corresponding to points having the same time average along trajectories for the x-component of velocity, u^*.
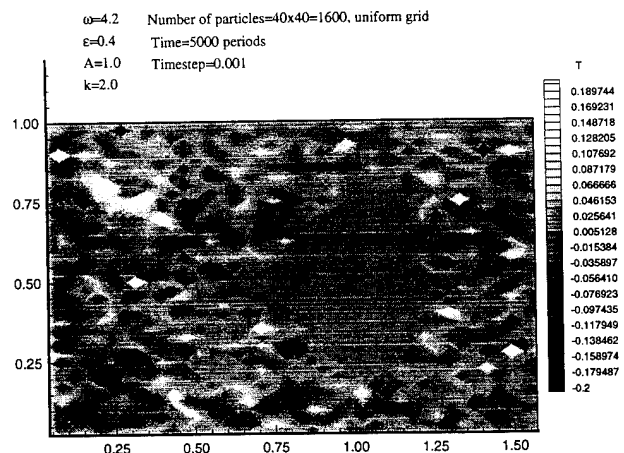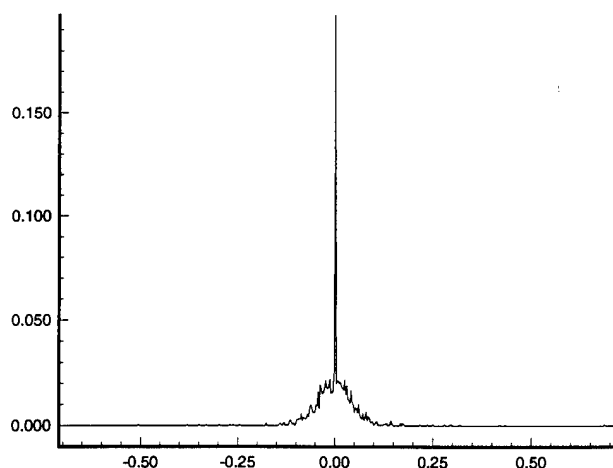
The distribution of the average x-component of velocity.

The nature of the coefficient a gives some insight into the dynamical mechanism giving rise to t^2 dispersion. It is easy to see that since the expression inside the angle brackets defining a is nonnegative, $a=0$ if and only if $u^* = <u^*>$ on the support of p, i. e., on the set of points for which $p(x, z, \theta)$ is *nonzero*, with the possible exclusion of sets of measure zero. However, $<u^*>$ is a constant. Therefore, we can make the following conclusion. Let $C \subset D$ x S^1 denote the support of $p(x, z, \theta)$. Then, if $u^*(x, z, \theta)$ is not constant almost everywhere on C, $D_x(t)$ t^2 as $t \to \infty$. Now assume that the flow is ergodic. Then $u^*= <u^*> = <u>$ almost everywhere. Therefore, $a=0$. So, a necessary condition for t^2 dispersion is non-ergodicity of the flow.

We end with some final observations.

1. Note that our result is independent of the Reynolds number. We are dealing solely with kinematical considerations.

2. There has been much work done in the last 10 years on chaotic fluid particle dynamics in two dimensional, time-periodic velocity fields. In such situations one typically sees a mixture of regular and chaotic regions of fluid particle motions in the flow. Our dispersion result implies that if one takes an initial distribution of points that is, roughly speaking, not entirely contained in a *single* regular or chaotic region, then the asymptotic behavior of the dispersion will go like t^2.

3. The case of a *diffusive* tracer has recently been treated by Mezic' *et al.* [1994]. This work shows that the t^2 dispersion result in the non-diffusive case is important for studying the diffusive case in the high Peclet number limit. (The Peclet number is a dimensionless number that is typically of the form $Pe = \frac{Ul}{D}$, where U is a charac-

teristic velocity, l is a characteristic length, and D is the diffusivity.) In particular, for the time-periodic cellular flow it is possible to show that t^2 dispersion of the convective part of the problem implies a Pe^2 dependence of the effective diffusivity coefficient in the diffusive case. In fact, the dependence of the effective diffusivity on the Peclet number can be determined solely on the knowledge that the convective part of the problem exhibits t^2 dispersion. Numerical studies of chaotic incompressible flows typically show regions of chaotic and ordered behavior, therefore non-ergodicity. In order to study dispersion in chaotic regions, the usual procedure is to consider an initial distribution of points that is entirely contained in what seems to be a chaotic (and supposedly ergodic) region. From the above result, in the diffusive case it would not make any difference whether the points were initially placed in only one ergodic region, or spread out over several ergodic regions. The only importance lies in the fact that in the related non-diffusive problem, when the particles are placed initially in several ergodic regions, the nondiffusive dispersion behaves like t^2 at large times. Then the Pe^2 regime is obtained in the diffusive problem. In this context we consider these results to be typical for a large class of laminar flows.

Relative Time Scales of Lobe Transport Versus Transport by lecular Diffusion through Lobe Geometry

So far, we have seen how, in the absence of molecular diffusion, lobe dynamics can be used to quantify the spreading of a passive tracer for *finite times*. Also, we have seen how ergodic theory can enable us to understand the asymptotic (in time) behavior of dispersion. In this section we show how the lobes can be used to determine a time scale over which lobe transport dominates molecular diffusion. Our knowledge of the dynamics of fluid particles associated with lobes suggests the following criterion that might explain the time scale over which lobe transport dominates molecular diffusion.

The time scale, T_d, for a tracer to diffuse across a distance of the order of a turnstile width should be long compared to the time it would take for a lobe to be mapped across the boundary of a region, i. e. T.

Hence, we have

$$T_d = \frac{(\bar{d}(\varepsilon))^2}{D}$$

where $\bar{d}(\varepsilon)$ is the maximum width of a turnstile lobe. Using the $\sigma(\varepsilon)$ approximation to the turnstile width given by the Melnikov function, we have

$$\frac{T_d}{T} = \frac{(\varepsilon \frac{\omega}{A} sech(\frac{\omega}{2A})cosh(\frac{\pi^2 A}{2\omega})^2)}{TD}$$

According to our criterion, lobe transport will dominate diffusive transport provided $T_d \gg T$. We check this for certain parameter values. With $D = 5.0 \times 10^{-6} \frac{cm^2}{s}$ and A= 0.1 we have the following three cases:

1. $\omega = 0.6, \varepsilon = 0.1$ implies $T_D \approx 200T$,

2. $\omega = 0.24, \varepsilon = 0.1$ implies $T_D \approx 300T$,

3. $\omega = 0.6, \varepsilon = 0.01$ implies $T_D \approx 2T$,

Thus, in the first two cases we would expect lobe transport to dominate molecular diffusion for about 200 and 300 periods, respectively, and in the last case only for about 2 periods. This can be check by considering the generalized Langevin equations, which describe the influence of molecular diffusivity:

$$\dot{x} = -\frac{\partial \psi}{\partial z} + \eta(t), \qquad (9)$$

$$\dot{z} = \frac{\partial \psi}{\partial x} + \zeta(t), \qquad (10)$$

where $\eta(t), \zeta(t)$ (diffusion terms) are random variables with a Gaussian probability distribution , such that their correlations are:

$$<\eta(t)\eta(t')> = <\zeta(t)\zeta(t')>=2D\delta(t-t'), \quad (11)$$

$$<\eta(t)\zeta(t')> = 0. \qquad (12)$$

In Figure 8 we compare the results of the lobe dynamics calculations (solid lines), which were obtained by numerically implementing the procedure described in Section 5, and the calculations which consider molecular diffusion(dashed lines), which were obtained by integrating (10). From this figure we can see that our criterion works reasonably well. Thus we see that geometrical and dynamical features of the lobes have lead us to a physical argument that gives us a time scale on which molecular diffusion can be neglected in the process of inter-cell transport.

"Patchiness" in Fluid Flows and Distribution Functions

Finally, we want to describe a new phenomenon that may prove to be a useful way of describing flows in a variety of geophysical settings. Pasmanter [1988], [1991] has studied mechanisms that give rise to the variability of dispersion processes in the ocean. A particularly important phenomenon to which he referred is known as "patchiness", i. e. , a situation where parts of a distribution of passive tracer may disperse at different speeds compared to its surroundings. We want to show that the mathematical framework developed in Mezic' and Wiggins [1994c] can be useful for studying this phenomenon. We will illustrate this with the cellular flow example.

In the cell-to-cell transport problem the time average along particle trajectories of the x-component of velocity is a useful quantity. In order to illustrate the "patchiness" effect we numerically determine the distribution of average x-components of velocity for fluid particle trajectories in one cell. In Figure 9 we plot contours corresponding to initial points of trajectories that have the same average x-velocity which we obtained by numerically computing these time averages for a uniform grid of 1600 points for a time interval of 5000 periods. Regions of nonzero average x velocity correspond to "accelerator modes", i. e., regions of initial conditions corresponding to trajectories with nonzero average velocity in the x direction, and these are the points that participate in cell-to-cell transport. In Figure 10 we plot a histogram of this data, i. e. , we plot the number of points corresponding to a given "bin width" of average x velocity, where the bin width is 0. 002. "Patches" are mathematically defined as sets of positive measure in the flow on which the x component of velocity has a constant time-average along fluid particle trajectories. In Mezic' and Wiggins [1994c] a distribution function is derived that allows one to deduce certain properties related to the patchiness. In particular, the "patches" correspond to points of discontinuity of a certain distribution function. An additional result obtained through study of this distribution function tells us that there are either a finite number of patches, or there is a countable number of them, but also countably many of them are of smaller measure than any prescribed number. In Figure 9, the "patches" are represented by the darkest and brightest spots. We could also define "patchiness" as the regime in which more than one "patch" exists. It then turns out that non-ergodicity of the flow is a necessary condition for "patchiness". More precisely, it can be shown that if the flow is ergodic, there is only one "patch", represented as one and only point of discontinuity of the distribution function derived in Mezic' and Wiggins [1994c]. Figure 10 represents the "generalized derivative" of this distribution function, that is, the peaks correspond to different "patches". From these results one can deduce a criteria for determining when a flow will be "patchy" If the flow is such that it has an ergodic component of positive measure, and if the initial distribution of passive tracer is such that the measure of that component is also of positive measure, then the flow will evolve into a "patchy" flow.

Summary

In this article we have taken a specific flow and shown how an arsenal of newly developed techniques from dynamical systems theory can be brought to bear on the study of the

Lagrangian transport properties of this flow. This dynamical systems approach shows much promise in dealing with the types of Lagrangian transport issues that arise in geophysical fluid dynamics. Much of the promise lies in the fact that the mathematical framework of dynamical systems theory is remarkably similar to the experimental framework of modern flow visualization (from, e. g. , tracer data or satellite observations) in that each is concerned with the motion in time over large regions of space and the role that lower dimensional organized "structures", or geometrical features, in space play in governing the motion. Dynamical systems theory provides a mathematical framework for quantifying and describing the effects of these low dimensional "organized structures" on Lagrangian transport. Consequently, this type of mathematical approach should prove ideal for analyzing transport and mixing processes associated with the large scale, organized motions observed in geophysical flows.

The mathematical development of dynamical systems theory is also being influenced by studies of Lagrangian transport problems in geophysical fluid dynamics. The flow studied in detail in this article was two-dimensional and time-periodic. Clearly dynamical systems techniques for three-dimensional time-dependent flows must be developed if these methods are to have large impact on Lagrangian transport issues. In this setting, a variety of new mathematical issues must be addressed. The beginnings of the development of this theory can be found in Beigie *et al.* [1991], [1992], [1994], Mezic′ and Wiggins [1994], and Wiggins [1992].

Finally, we mention a possibly revolutionary new development for Lagrangian transport problems. When the dynamical systems techniques are developed so that they can be coupled with modern computational methods for computing velocity fields the applicability of the methods will be greatly extended, as well as be more accessible to geophysical fluid dynamicists. Over the past 15 years computational fluid dynamics has developed into a subject in its own right. Now we have accurate algorithms for solving the Navier Stokes equations in a variety of physically important settings. However, many problems related to mixing and transport begin once this step has been accomplished. That is, first a solution to the Navier Stokes equations must be obtained in order to study the transport and mixing properties associated with that velocity field. In the vast majority of situations arising in applications, this solution can only be obtained numerically. Thus, we only have a numerical representation of the velocity field. Nevertheless, many dynamical systems results do not care about the specific analytical form of the dynamical system under consideration. Rather, they require that only certain *geometrical features* be present. For example, the existence of stable and unstable manifolds of some invariant set requires only the existence of a hyperbolic invariant set and the existence of Smale horseshoe type chaos requires only the transverse intersection of the stable and unstable manifolds of a hyperbolic

periodic orbit. Currently our research is focused on developing the theory and algorithms needed to perform dynamical systems type analysis with numerical representations of vector fields.

Biography

See *Profiles in Science.*

References

1. Arnold, V. I. and A. Avez [1968] **Ergodic Problems of Classical Mechanics.** Benjamin: New York.

2. Beigie, D. Leonard, A. and Wiggins, S. [1991] Chaotic Transport in the Homoclinic and Heteroclinic Tangle Regions of Quasi-periodically Forced Two Dimensional Dynamical Systems, Nonlinearity, **4**, 775-819.

3. Beigie, D., Leonard A., and S. Wiggins [1992]. The dynamics associated with the chaotic tangles of two-dimensional quasi-periodic vector fields: theory and applications, in **Nonlinear Phenomena in Atmospheric and Oceanic Sciences (IMA Volumes in Mathematics and its Applications - Volume 40).** Editors G. F. Carnevale and R. Pierrehumbert (Springer-Verlag: New York, Berlin, Heidelberg) 47-138.

4. Beigie, D. , Leonard, A. , and S. Wiggins [1994] Invariant Manifold Templates for Chaotic Advection. *Chaos, Solitons, and Fractals*, 4(6), 749-868.

5. Bolton, E. W. , Busse, F. and Clever, R. M. [1986] Oscillatory Instabilities of Convection Rolls at Intermediate Prandtl Numbers. *J. Fluid Mech.* , **164**, 469-486.

6. Camassa, R. and Wiggins, S. [1991] Chaotic Advection in a Rayleigh-Bénard Flow. *Phys. Rev.* A, **43**, 774-797.

7. Chandrasekhar, S. [1961] **Hydrodynamics and Hydromagnetic Stability.** Dover: New York.

8. Clever, R. H. and Busse, F. [1974] Transition to Time-Dependent Convection. *J. Fluid Mech.* , **65**, 625-645.

9. I. Mezic′, I. and Wiggins, S. [1994a] On the Integrability and Perturbation of Three-Dimensional Fluid Flows with Symmetry, *J. Nonlinear Science*, 1994, 4(2), 157-194.

10. I. Mezic′, I. and Wiggins, S. [1994b]On the Dynamical Origin of Asymptotic t^2 Dispersion of a Non-Diffusive Tracer in Incompressible Laminar Flows, Physics of Fluids A, 1994, 6(6), 2227-2229.

11. I. Mezic′, I. and Wiggins, S. [1994c]Birkhoff's Ergodic Theorem and Statistical Properties of Chaotic Dynamical Systems, with Applications to Fluid Mechanical Mixing and Dispersion, submitted to Physica D.

12. I. Mezic′ , I. , Brady, J. and Wiggins, S. [1994] Maximal Effective Diffusivity for Time-Periodic Incompressible Fluid Flows, accepted for publication in the SIAM Journal of Applied Mathematics.

13. J. Ottino [1989]. **The Kinematics of Mixing: Stretching, Chaos, and Transport**. Cambridge University Press: Cambridge.

14. Pasmanter, R. [1988] Deterministic Diffusion, Effective Shear and Patchiness in Shallow Tidal Flows. In: Dronkers, J. and Van Leussen, W. (eds.) Physical Processes in Estuaries, pp. 42-52. New York:Springer-Verlag.

15. Pasmanter, R. [1990] From chaotic advection to chaotic Schrödinger-type equations. *Physical Review A*, **42**, 3622-3625.

16. Pasmanter, R. [1991] Anomalous diffusion and patchiness generated by Lagrangian chaos in shallow tidal flows. *Physics of Fluids A*, **3** (5), 1441.

17. Ridderinkhof, H. , and Zimmerman, J. T. F. [1992] Chaotic stirring in a tidal system. Science **258**, 1107-1111.

18. Solomon, T. H. and Gollub, J. P. [1988] Chaotic Particle Transport in Time-Dependent Rayleigh-Bénard Convection. *Phys. Rev. A*, **38**, 6280-6286.

19. Weiss, J. B. and Knobloch, E. [1989]Mass transport and mixing by modulated travelling waves. *Physical Review A*, **40**, 2579-2589.

20. Wiggins, S. [1992] **Chaotic Transport in Dynamical Systems**. Springer-Verlag: New York, Heidelberg, Berlin.

Profiles in Science
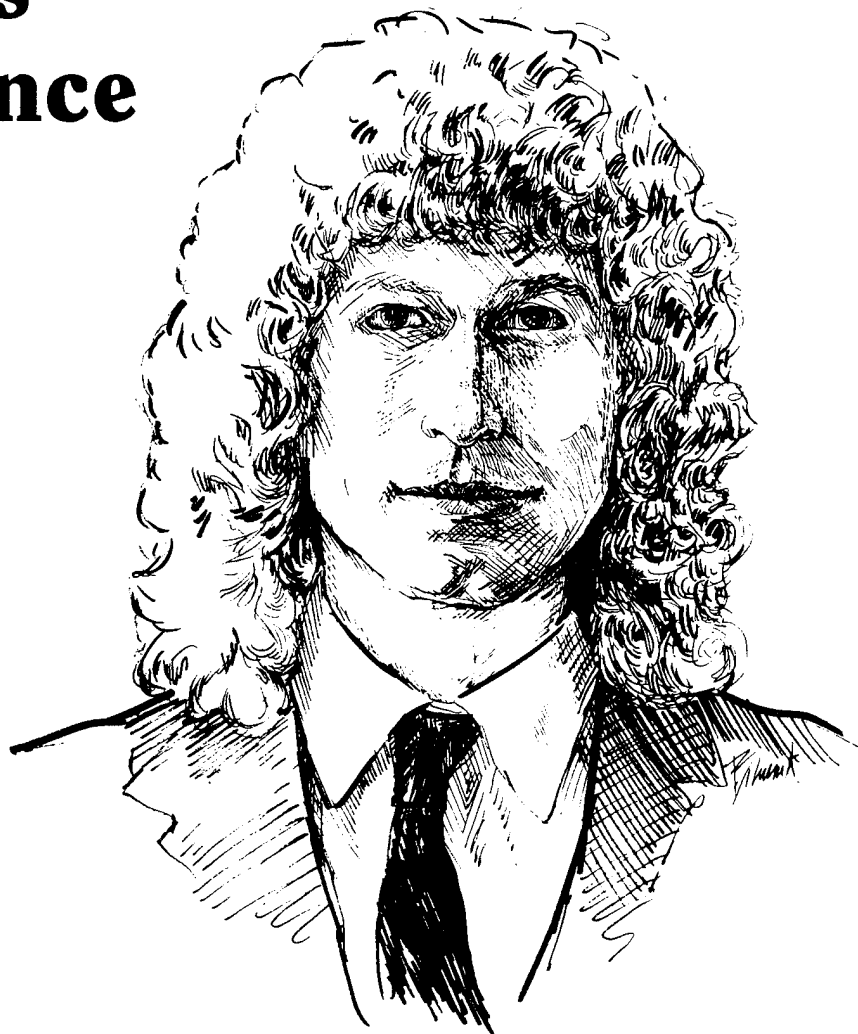
Stephen Wiggins

Stephen Wiggins is a Professor of Applied Mechanics and Control and Dynamical Systems at the California Institute of Technology and a Principal Investigator of the Office of Naval Research. His research interests and publications, which include five books, are in the areas of applied nonlinear dynamical systems and chaotic phenomena, with applications to fluid mechanics control theory, mechanical systems and theoretical chemistry. He is one of the founding editors of the *Journal of Nonlinear Science* and the magazine *Nonlinear Science Today*.

In the field of fluid mechanics, his current research is concerned with developing new techniques for studying convective mixing and transport problems from the geometric point of view of dynamical system theory. This type of mathe-

matical approach is proving to be ideal for analyzing transport and mixing processes associated with the large scale, organized motions observed in geophysical flows. A current direction of his research is involved with extending the dynamical systems techniques so that they can be coupled with modern computational methods for computing velocity fields. This should greatly extend the dynamical systems methods, as well as make them more accessible to geophysical fluid dynamicists.

In 1989, Professor Wiggins received an ONR Young Investigator Award in applied analysis as well as a National Science Foundation Presidential Young Investigator Award. In 1990 he was the Stanislaw M. Ulam visiting scholar at the Center for Nonlinear Studies at Los Alamos National Laboratory.

Settling and Chaotic Mixing in Oceanic Flows: the Rôle of Heteroclinic Orbits

C.K.R.T. Jones, G.Haller, P.D.Miller, J.Rubin
Division of Applied Mathematics
Brown University

1. Introduction

The difficulties involved in collecting data on oceanic motion are evident and the inherent uncontrollability of the ocean for experimentation presents a formidable scientific challenge to those seeking to understand it. The data that is collected from the tracking of strategically placed floats fits very well with the Lagrangian perspective on fluid mechanics, wherein motion is viewed through the following of fluid particles, as it is assumed that the paths of these floats reflect those of fluid particles. These Lagrangian trajectories are, from the dynamical systems viewpoint, the orbits generated by a vector field that is precisely the Eulerian velocity field of the fluid flow. This perspective thus offers a natural mathematical context through which to study questions about oceanographic flows.

However, this form of oceanographic data collection through the tracking of floats suggests a deeper reason for the suitability of the dynamical systems perspective. Since only a small number of SOFAR (or RAFOS) floats can be placed in areas of the ocean under study, and they can only be tracked for a certain period of time, usually a year or less, the resulting particle paths must be viewed as a sampling of the corresponding Lagrangian trajectories. The pictures of these float paths are put together to form what are commonly known as "spaghetti" plots, see Figure 1 for an example taken from reference 4. It is clear that we can only rely on general qualitative features of such plots for an assessment of the fluid motion. One cannot hope to give an explanation of detailed properties of these paths. Indeed, such an explanation would not be meaningful as any individual path is the inevitable victim of small-scale, temporary effects. However, the large-scale features of the paths that are present in a number of samplings should be explained.

The modern theory of dynamical systems, with its emphasis on qualitative properties and characteristic geometric features of trajectories, provides a fitting perspective on the issues raised by the study of oceanographic flows. The underlying tenet of geometric dynamical systems theory is that certain basic geometric structures can be isolated which organize the overall structure of the flow. In particular, certain specific trajectories, if they can be located, will demarcate different regions of qualitatively distinctive trajectory motion. Specifically, stagnation points of the flow and their attendant stable and unstable manifolds (sets of trajectories approaching the stagnation point in, respectively, forward and backward time) play definitive rôles in organizing the flow.

From the dynamicist's perspective, the oceanographic flow fields are presented to us on three levels of increasing accuracy, and complexity. The simplest level of model is of a velocity field that is postulated as an accurate model of the phenomenon under investigation. This will be formed, commonly, in terms of an unstable, or neutral, mode superimposed on a base flow. Such a flow leads to an analytic expression for an ordinary differential equation whose analysis is, in principle, possible by existing techniques and only restricted by its complexity, in particular its dimension. The next level of model is the numerical model which consists of a velocity field given as a numerical database that is constructed by solving the relevant partial differential equation on an appropriate domain. A dynamical systems approach to such a velocity field is severely impeded by the fact that all the developed techniques are based on the idea that the velocity field is supplied to the mathematician analytically. A new perspective is thus called for and the development of techniques for handling numerically generated velocity fields is a significant task that remains to be adequately addressed. In particular, the numerical determination of the relevant structures, such as stable and unstable manifolds, for numerical velocity field data sets is required. A strong case has been made by Ridderinkhof and Zimmerman[23], for the relevance of these dynamical structures in a numerical model of the Wadden Sea. The final level is the experimental data set available for the situation under investigation. These data sets, as discussed above, are usually based on the tracking of floats and, while insufficient to be viewed as a complete model, must always be used as the final arbiter of the success of a given piece of analysis.

In this review, we shall consider models at the first level. The formulation of such models as base flow plus perturbing mode can offer great insight into charcateristic flows that may truly exist as the nonlinear equilibration of such "neutral" or "unstable" directions from the base flow. Explicit analytic expressions, or even approximations, for such fully nonlinear Eulerian flow fields are comparatively rare, and these "linear" approximations offer, with the existing technology, the best way to make meaningful, analytic predictions about the nature of Lagrangian trajectory motion in the full flow field. However, a goal of the mathematical development motivated by oceanographic problems must be the construction of better analytic models that incorporate real nonlinear effects while remaining faithful to the underlying physics.

Our focus will be on heteroclinic orbits, which are trajectories joining different stagnation points, and are often known as separatrices on account of their function in separating different flow behaviors. We favor here the more modern term of "heteroclinic orbit" because the main point of the message is that, under perturbation, these structures no longer perform this function of separation. Nevertheless, there remain, typically, heteroclinic orbits after perturbation. We shall present three examples that illustrate how an elucidation of the structure of these orbits, in particular for small perturbations of the base flow, can reveal the mechanisms in the flow for the transport of particles.

The first example concerns the settling of a particle in a cellular flow field. The particle of interest here is not, in fact, a fluid particle but an aerosol particle, and a key point in the analysis is the small inertial effect experienced by such a particle. the question of interest is whether the particle under consideration can be trapped in the cell or continue to settle through the flow indefinitely.

An interesting feature of jets in the ocean, such as the Gulf Stream, is the spawning of rings that form a vortex motion, and this is the motivation for our second example.
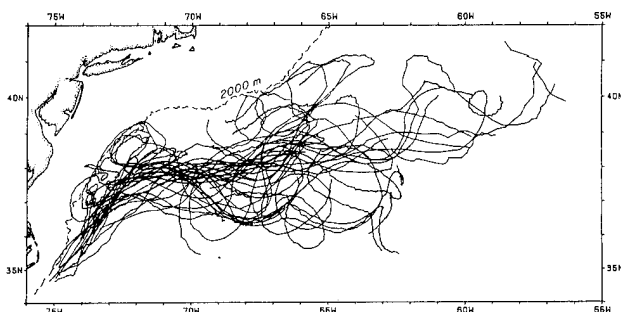
These rings carry, for instance, cold water into the region of warm water to the south of the Gulf Stream. They tend to travel in the reverse direction from the jet and survive for a significant amount of time, often until hitting the continental shelf. The formation of these rings is not well understood, see Pratt et al.[20] and many of their features remain to be explained. Kirwan et al.[16,18] formulated a model for such rings in terms of rotating modons. These are special solutions of the quasigeostrophic equations and their mixing properties will be discussed in section 3.

The third example concerns the transport of water within, and across, an oceanic jet. The general mechanisms for mixing across a jet, such as the Gulf Stream, are of fundamental importance. Various kinematic models have been formulated for the clarification of this transport, but, recently, models of velocity fields that are dynamically consistent have been derived by Pratt et al.[21] We discuss in section 4 some of the issues involved in the transport of fluid across such a jet.

In each of these examples, there is an "unperturbed" flow field that is a one-degree-of-freedom Hamiltonian system. The distinguished orbits that connect stagnation points to each
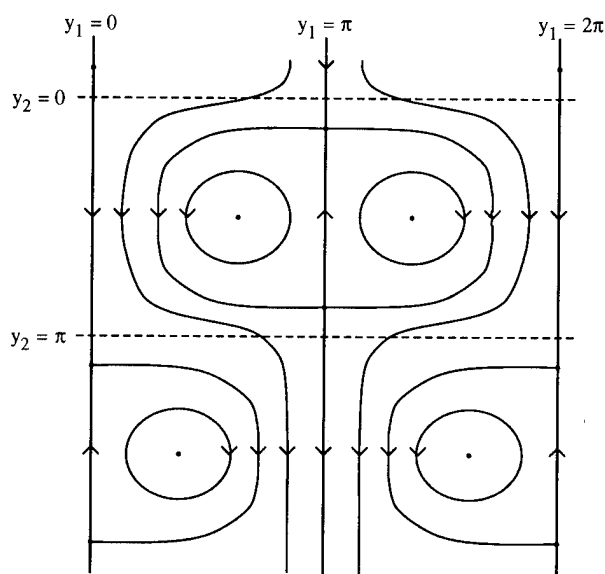
SPAGHETTI DIAGRAM OF RAFOS FLOATS
1984—1985

Figure 2.

other separate regions of contrasting Lagrangian motion from each other. The perturbations supplied by effects unaccounted for in the base flow will tend to break these separating orbits and offer the possibility of transport between regions that were, in the unperturbed case, characterized by different motions. We shall see, in each of the examples discussed below, the implications of the perturbations on these distinguished orbits.

2. Settling in a Cellular Flow Field

The problem of whether particles of non-fluid matter settle in the ocean under the influence of gravity is obviously of great importance. A cellular flow field is a model of Langmuir circulation and we consider here the issue as to whether aerosol particles will tend to settle through such a flow field or be trapped and recirculate within that cell. A key point is the rôle of the inertia of the particle in question. The inertial effects can provide, as will be seen below, an effective dissipation of the Hamiltonian that arises as the streamfunction of a 2-dimensional incompressible flow.

The settling of an aerosol particle through a cellular flow field was studied by Stommel[27]. Stommel's analysis neglected the inertia of the particle, and thus the particle was effectively treated as a fluid particle settling through the flow field under the combined influences of gravity and the surrounding fluid.

He showed that, in this scenario, both trapping and settling were possible. Indeed, the ratio of trapped particles to settling particles varied with the characteristic terminal settling velocity due to gravity. In physical space, when the influence of inertia is omitted, heteroclinic orbits to the stagnation points on vertical invariant lines between cells separate the regions from which particles will settle from those in which particles will be trapped, as shown in Figure 2.

Indeed, these heteroclinics form invariant, protected pods. Under the periodic velocity field, the Lagrangian trajectories outside a pod will settle through all of the cells they enter, whereas the Lagrangian trajectories inside a pod will be trapped forever.

Despite the apparent possibility of many particles being suspended in the cells, Maxey and Corrsin[15,14] observed, based on numerical experiments, that inertial particles had a greater tendency than fluid particles to settle. The true problem with inertia included is, however, a perturbation of that considered by Stommel, and we must consider whether any analogue of the protected pod, which might guaranteee the suspension of particles, exists in the inertial problem.

If the inertia of the particles moving through the cellular flow field is small, but nonzero, the velocity field for these particles becomes a singularly perturbed version of that for fluid particles acted upon by the cellular flow field and gravity. The analysis and interpretation of such singularly perturbed problems contains many pitfalls. Fortunately, a technology exists which can render a complete geometric description of the trajectories of such perturbed systems, and it can be invoked here to give a clear and unambiguous answer as to whether, under the influence of inertia, particles will prefer to settle or not.

This set of techniques is based on a striking collection of theorems due to Fenichel.[7,8,12] These results give conditions under which, for the perturbed system, there exists an invariant manifold (a smooth surface of solutions) that carries a vector field which is a small (regular) perturbation of the formal limit equation.

If we let y(t) denote the position of the center of the particle in space (y=(y_1,y_2)) and take the downward direction to be the direction of positive y_2 (the opposite of the convention in reference 11) then the equations of the following model govern the motion of an aerosol particle in a cellular flow field

$$\dot{y} = v_1$$

$$\dot{y} = v_2$$

$$\varepsilon \dot{v}_1 = -v_1 + \sin y_1 \cos y_2$$

$$\varepsilon \dot{v}_2 + -v_2 - w - \cos y_1 \sin y_2 \qquad (1)$$

Here, v(t) is the velocity of the particle and W is the settling velocity scaled so that $0 < W < 1$. The small parameter

Here, v(t) is the velocity of the particle and W is the settling velocity scaled so that $0 < W < 1$. The small parameter $\varepsilon > 0$ is the Stokes number and measures the inertial response time of the particle to the medium. The case $\varepsilon = 0$ renders the formal limit in which the particles have no inertia and behave merely as fluid particles. Fenichel's work implies that there exists, for system (1) with small inertia, an invariant manifold of the type discussed above. This invariant manifold, known as the slow manifold, is given by a small perturbation of the algebraic conditions found by formally setting $\varepsilon = 0$ in the last two equations of (1). An application of Fenichel's further results combined with some simple dynamical systems arguments show that, in this case, the slow manifold is actually globally attracting. Thus the asymptotic motion of all Lagrangian trajectories will be determined by the vector field on the slow manifold.

A key point to notice is that the slow manifold is parametrized by the physical space variables (y_1, y_2). To analyze the true behavior on the manifold, it is necessary to calculate the $O(\varepsilon)$ terms in the perturbed vector field. This is achieved by using the invariance property of the manifold and the full equation itself. The resulting system on the slow manifold is

$$\dot{y}_1 = \sin y_1 \cos y_2 - \varepsilon \sin y_1 \, (W \sin y_2 + \cos y_1) + O\,(\varepsilon^{\,2})$$

(2)

$$\dot{y}_2 = - W - \cos y_1 \sin y_2 + \varepsilon \cos y_2 \, (W \cos y_1 + \sin y_2) + O(\varepsilon^2).$$

As commented above, the long-time behavior of aerosol particle trajectories is determined completely by the trajectories of this vector field. Moreover, the interpretation of these trajectories is considerably facilitated by the fact that the dependent variables in (2) are exactly the space variables. Setting $\varepsilon = 0$ in (2), we recover the velocity field for fluid particles, the trajectories of which are sketched in Figure 2. We are now ready to address the key question as to whether particles should be expected to settle under the influence of the vector field (2). The answer will obviously come from studying the fate of the pods present in the $\varepsilon = 0$ system under the perturbation supplied by the $O(\varepsilon)$ terms of (2). This is tantamount to asking how the heteroclinic orbit surrounding the pod in the interior of each cell will break under the influence of this perturbation (the vertical heteroclinic stays in place). A few simple sketches will convince the reader that if the unstable manifold falls outside the stable manifold then the process of settling is facilitated, whereas the reverse configuration would result in more trapping. The determination of the direction of breaking of heteroclinic orbits is the objective of Melnikov calculations,[10,30] and the issue can be resolved by calculating the sign of a certain integral. This integral presents many technical difficulties, and we do not evaluate it directly, but it can be shown analytically that its actual sign corresponds

to the unstable manifold falling outside the stable manifold. This indicates a strong enhancement of settling[11].

In this way, we show that any small inertial effects in fact force particles to settle through a cellular flow field and make the probability of suspension almost non-existent.

Figure 3 provides a sketch of the resulting flow of particles with small nonzero inertia.

It is also shown analytically in reference 11 that certain characteristic paths emerge in the slow manifold, along which the aerosol particles will, asymptotically, congregate and travel. This corroborates further numerical observations due to Maxey and Corrsin.[15,14]

Although the underlying cellular flow field is a reasonable model in certain oceanographic circumstances, it is, of course, very idealized. Nevertheless, our work shows that the inclusion of inertial effects, if properly interpreted on a slow manifold, supplies an effective dissipation of the Hamiltonian streamfunction. Such effects are also seen in recent related work of Tio et al.[28], in which settling through a critical layer is studied. This may partly account for observations in which particulate matter in the ocean is seen to collect in certain well-defined areas[29,32], despite the fact that it is under the influence of a time-dependent, incompressible, almost stratified flow, which one would otherwise expect to be strongly homogenizing.

3. Rotating Modons

In recent work, Mied, Kirwan and Lindemann[16] have proposed rotating modons as models of rings that result from

---

Figure 3.

The trajectories of those particles lying on the slow manifold are depicted here. Other trajectories will asymptotically approach this configuration. Small inertia is included and has the effect of breaking the heteroclinic orbits in such a way as to force settling. Particle paths do not become trapped and those lying within the protected pods in the zero inertia case can leak out and settle.
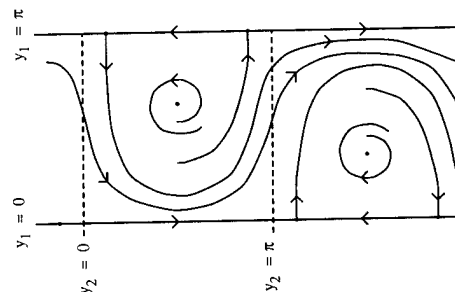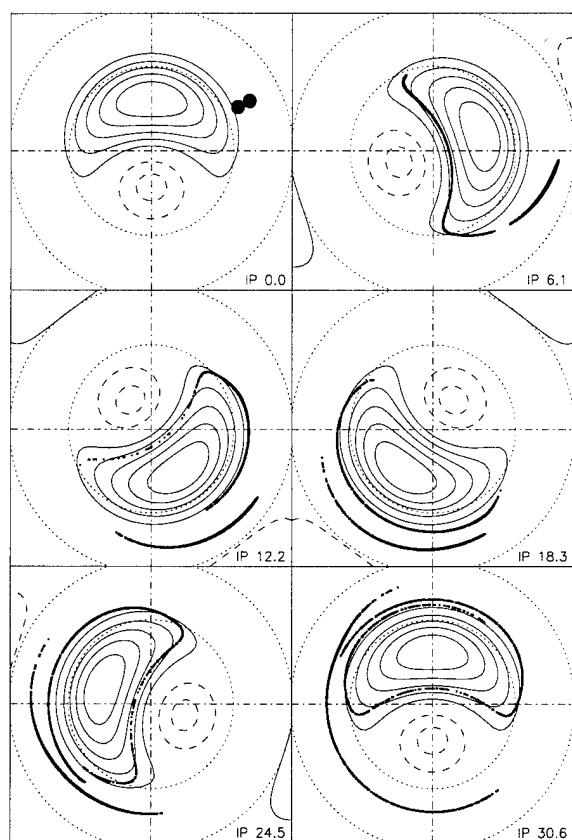

Figure 4.

Hamiltonian (effective streamfunction) of the feature model for 82-B. Solid and dashed curves are positive and negative values, respectively. The contours have been normalized by a convenient plotting scale. The dotted circles show model scale lengths for the upper and lower model layers. The inner circle radius is 120 km. There are two types of critical points in this plot. The three diamonds depict stagnation points that are local extrema. There are two dots near the tips of the SP contour lines. These are saddle points. The SP contour is the value of teh Hamiltonian at the saddle points.

have the effect of trapping the modon and preventing it from lateral movement, see[18]. Of particular interest are dipolar vortices in which two regions of opposite rotation are matched together. It is suggested in reference16 that such dipoles model pairs of warm and cold cores that are attached to each other, and can even become so attached as the result of a collision. Of interest in our study is the local mixing properties of such modons. For instance, is it possible that fluid from outside the modon can be mixed into it? Can it flow into the core? Or between the two complementary cores? If not, what external mechanisms might facilitate such mixing?

The rotating modons are solutions of the quasigeostrophic equations of a prescribed form. They are constructed by finding solutions in different circular regions and matching at the boundaries. This is quite a complicated procedure that leads to formidable calculations for solutions of the resulting partial differential equations.

In the paper by Kirwan et al. [18], each layer is divided into an inner (circular) modon region and an outer region. The radii of the regions in each layer will, in general, be different. The quasigeostrophic equations for the potential vorticity q_i and the streamfunction ψ_i are assumed to hold in the regions of each layer, $i = 1,2$, with appropriate matching conditions at the boundary. Solutions of these equations which are steady in a rotating frame of frequency ω can be found under the ansatz that the effective streamfunction

Figure 5.

This vortex system has a rotation period of 30.6 inertial days. Positive values are depicted as solid curves and negative values as dashed curves. Two blobs are initialized on either side of a saddle point; the red blob is just inside the saddle point while the blue blob is just outside. The blob radii are 5km and there is a 2 km distance between the blobs.

the pinching off of vortex-like regions from such jets as the Gulf Stream. These multipole vortex systems consisting of one or more cyclonic eddies moving around an anticyclonic ring often are seen in AVHRR imagery in the coastal/open ocean interface. The nonlinear feature model developed by Kirwan et al.[18] accounts for many of the charcteristics seen in the imagery. These modons are specific solutions of the quasigeostrophic potential vorticity equations for a 2-layer model, in such a setting they were first introduced by Flierl et al.[9]. Modons are steady in a frame that is rotating at a fixed frequency. Bottom topography can be included, and this can
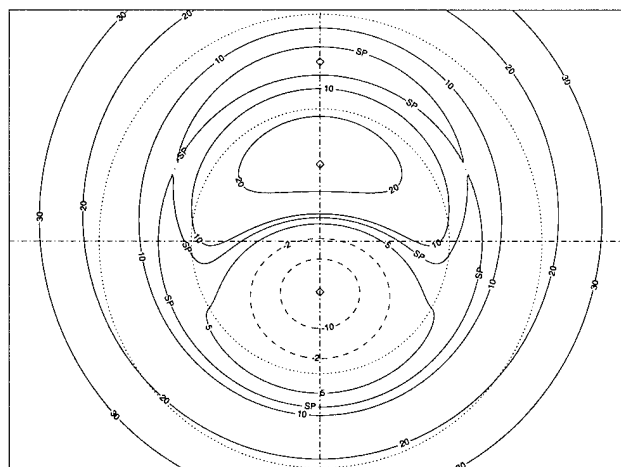
Figure 6.

Flow associated to the single cusp jet model with a single neutral mode superimposed. When viewed in a reference frame moving with the speed of the neutral wave, the flow is time-independent and admits two rows of critical points at the steering lines. Fluid between the steering lines moves to the right as its speed is greater than the speed of the reference frame, and fluid outside the steering lines moves to the left. In each of the figures of this section, the heteroclinic orbits are colored red (blue) for the pieces that are generated as unstable (stable) manifolds. This is not so meaningful in the unperturbed case (Figures 6, 7 and 9) since, on the heteroclinic orbits the stable and unstable manifolds coinicide. the reamining trajectories are colored red.
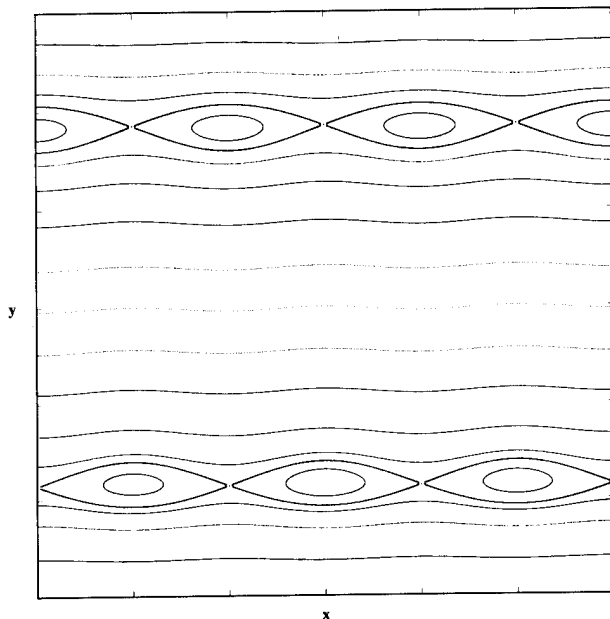
$$Y_i = \psi_i - \frac{\omega r^2}{2}$$

and the potential vorticity are functionally related, with a different relation in each layer and region. The quasigeostrophic equations are then

$$J(Y_i, q_i) = S_i,$$

where S_i are sources at the boundaries of the regions to compensate for the jumps in potential vorticity. The relevant solutions are then found by Kirwan et al.[18] from solving the partial differential equations coming from the functional relations.

In physical variables, namely r, θ and t, the Lagrangian trajectories are those of a Hamiltonian system with time-dependent forcing. There are two such systems, one for each

layer, and the Lagrangian trajectories in each layer are independent of those in the other layer, although the corresponding streamfunctions are not. Within each layer the Lagrangian trajectories are the same for any depth. The trajectory equations are then

$$\frac{dr}{dt} = \frac{1}{r} \frac{\partial \psi_i}{\partial \theta}$$

$$\frac{d\theta}{dt} = \frac{1}{r} \frac{\partial \psi_i}{\partial r}, \tag{3}$$

where the streamfunction $\psi_i = \psi_i(r, \theta - \omega t)$. The streamfunction will be continuous across the boundaries of the various regions, but not necessarily smooth. Since the system (3) is a time dependent Hamiltonian system, its trajectories can be, ostensibly, chaotic. However, if viewed in a rotating frame, it is easily seen that the effective Hamiltonian Y_i becomes a time independent Hamiltonian and after the appropriate changes of coordinates, (3) can be recast as a one-degree-of-freedom Hamiltonian system. We introduce the variables $\Theta = \theta - \omega t$ and a scaled time τ, so that (3) becomes

Figure 7.

Increasing the wavenumber of the neutral mode draws the steering lines closer to the centerline of the jet and the meander of the jet becomes more pronounced. The assymetry in the cat's eyes is due to the exponential form of the eigenfunctions. Here the neutral mode has wavenumber $k = 8$ and amplitude $a = 0.01$.
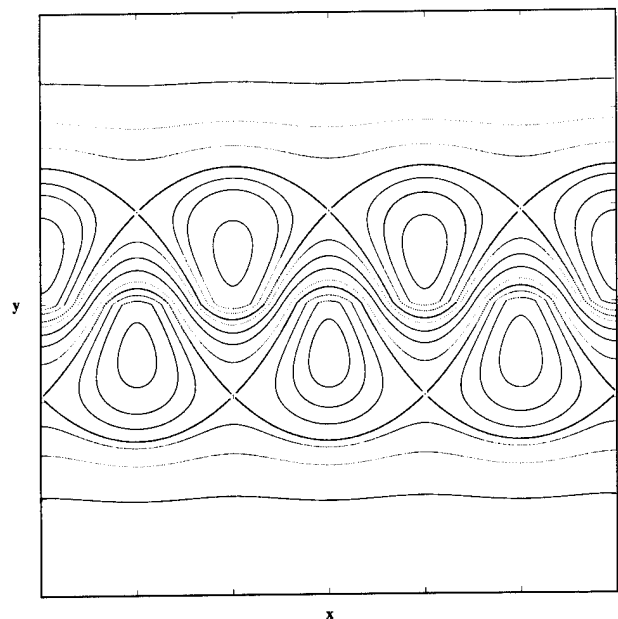
Figure 8.

Adding a second neutral mode to the jet model results in a time periodic vector field. Here the second mode is moving faster than the first mode with wavenumber $k_2 = 16$ and amplitude $\varepsilon = 0.001$. In the presence of this time periodic perturbation the heteroclinic orbits break up into transverse intersections of the stable and unstable manifolds for the associated Poincare map. The most significant mixing occurs on the inside of the jet, however, no mixing occurs across the body of the jet. The color coding (red-unstable, blue-stable manifolds) shows clearly the intermingling between stable and unstable manifolds on the inner heteroclinic orbits.
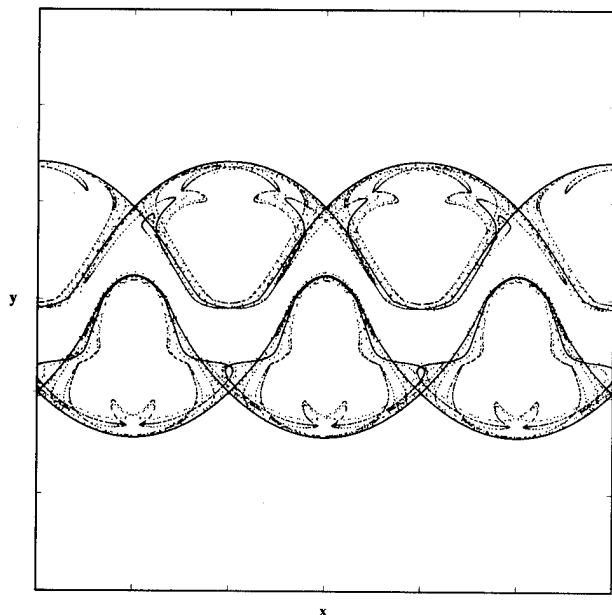
$$\frac{dr}{d\tau} = -\frac{\partial Y_i}{\partial \Theta}$$

(4)

$$\frac{d\theta}{d\tau} = \frac{\partial Y_i}{\partial r}$$

where the right hand side depends only on the phase space variables r and Θ.

This casting of the problem has rather striking implications. If the modon is viewed in the rotating frame, then the trajectories must follow the contours of the effective Hamiltonian and are, in particular, quite tame. We shall focus on the case of a dipolar modon. In recent, and ongoing, work Kirwan and the authors have discovered stagnation points in the flow field (3) for the upper layer. These correspond to periodic

Lagrangian trajectories in physical space. These stagnation points are crucial in understanding the dynamics of (3). Indeed they are located near the edge of the modon boundary (radius of inner region) for the upper layer. The outer ring of heteroclinic orbits (called a heteroclinic cycle) surrounds both the cyclonic and anti-cyclonic vortices (warm and cold cores) of the modon. The inner cycle surrounds only the cyclonic vortex. Figure 4 shows the qualitative nature of the phase portrait of (3). The figure is based on data for a model of 82-B, using hydrographic and AVHRR data. This data is well documented in Kenelly et al.[17] The two stagnation points are located in the north-east and north-west sides of the modon structure. The heteroclinic orbits are contours of the effective Hamiltonian joining the stagnation points. These are not cpatured exactly in the Figure 4, but reasonable approximations can be seen in the contours marked SP, it is left to the readers imagination to see how these are connected to the saddle stagnation points to form the heteroclinic orbits. Of particular significance in this analysis is that the heteroclinic cycles provide a barrier to the mixing of fluid in certain regions. The outer homoclinic cycle prevents any outside fluid from infiltrating the modon structure. This is not obvious from pictures in the physical space as this homoclinic orbit will not be circular and hence will change position as the modon rotates. Nevertheless, if a fluid particle is outside the rotated version of this cycle at an appropriate time, the modon flow will never carry it through the modon. In some sense, this cycle defines the modon as it supplies the modon boundary. The inner heteroclinic cycle provides the barrier between the two main vortices of the modon. It should be noted that the contouring of the effective streamfunction (Hamiltonian) has uncovered a third vortex patch which was somewhat unexpected. It is, however, viewed as less signifi-cant than the two primary vortices.

A numerical experiment, performed by B.Lipphart (Old Dominion University), gives clear corroboration of the protection of the modon by the outer heteroclinic cycle. In this numerical experiment, shown in Figure 5, two blobs of initial data are placed in locations near the northeasterly stagnation point. The outer blob (blue) is placed just outside the outer heteroclinic cycle at the stagnation point, and the inner blob (red) just inside. The resulting particle paths are then strobed at six, equally spaced, time intervals in physical space ending after one period. The contour lines sketched in Figure 5 are those of the original streamfunction (ψ_t and not Y_i) and their presence is used to facilitate the viewing of the modon. The different fates of the two blobs can be seen quite clearly from the numerical plots. Indeed, the blue particle paths are kept out of the modon structure, while the red ones are sucked into the region between the vortices. This difference is especially striking when one considers that the initial separation of the blobs is not that great, only about 2km. in physical space.

In the real oceanographic systems, one cannot expect the modons to be totally protected from the outside fluid. Indeed,

the outside fluid will be sucked through the center of the modon and, to some extent, into the edges of the vortices. The question then arises as to what perturbing mechanisms might effect such mixing of fluid through the modon structure. This is the subject of our ongoing work in collaboration with Kirwan, but some observations can be made as to why and how we anticipate this being realized. The outside ocean is a ready supplier of perturbations that will manifest themselves as time varying influences on the modon structure. It is a well-known fact in dynamical systems that for area-preserving systems, homoclinic orbits for the associated Poincaré map will persist under perturbation. This can be applied here but, since the perturbed system will be time-dependent, has the consequence that the stable and unstable manifolds of a fixed point, close to the original stagnation point, will intersect. Since these are now invariant manifolds for a map, their intersection produces a quite different scenario. Indeed, the manifolds for the perturbed system should intersect transversely, which we expect as a consequence of a symmetry argument similar to that noted in the following section, and chaotic mixing of fluid particles between the regions that were previously protected from each other is now likely,[31]. It may be commented here that the conservation of potential vorticity will prevent chaotic mixing, as observed recently by Brown and Samelson[5]. However, in the unperturbed case, the poten-tial vorticity and effective streamfunction are linearly dependent, that is indeed how they were found for the modon, and thus the analysis of reference 5 does not apply in this case. Even though we expect mixing through the modon to occur under such time-dependent perturbations, the KAM Theorem, see reference 1 for instance, can be applied to show that, under small perturbations, some of the orbits surrounding the vortex regions will survive as invariant tori. This will protect the vortices themselves from being sucked into the mixing process. Thus, we expect for the flow that fluid will be mixed through the modon, that is to say between the two vortex cores, but not into the cores themselves.

A key point here is how to model the time dependent perturbation, whether by a superimposed mode or a time variation of parameters in the problem, such as the radii of the regions in one of the layers. Issues of dynamical consistency and physical relevance are of central importance. However, we expect that mixing of fluid will occur through the modon for almost all such perturbations. Given the formulation of an appropriate model, mixing rates can even be calculated from the Melnikov function, as formulated by Rom-Kedar and Wiggins[24,31], and for some more recent theory[25], and the different mechanisms available can be compared for the efficacy in the process of mixing through the modon.

Figure 9.

*Modeling the dynamics at a steering line where
U'(y) = 0. Here the steering line occurs at a point where the base velocity profile attains a minimum (U'' (0) 0). Because of the scaling in this analysis the dynamics actually occur over a smaller range of y than in the previous figures.*
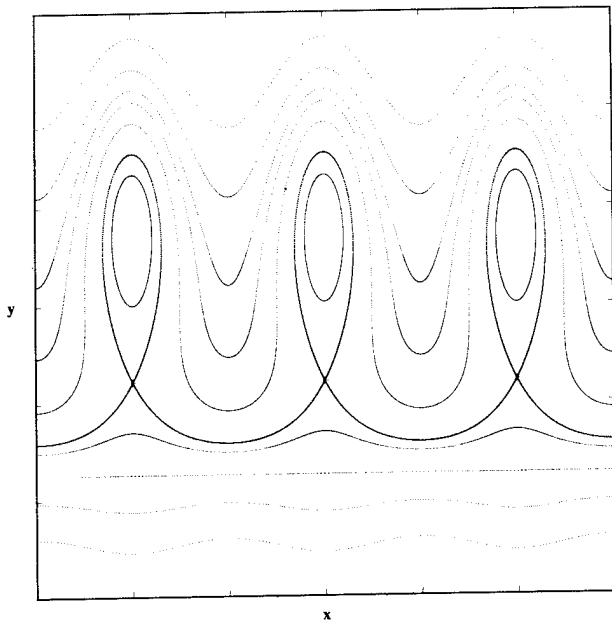

4. Mixing across Jets

The mechanism for the transport of fluid particles across such oceanic jets as the Gulf Stream is not well understood. Near the surface the presence of high potential vorticity gradients at the center of the jet appear to act as barriers to this transport. Indeed, this has been experimentally corroborated by Behringer, et al.[2]. Nevertheless, it appears to occur either by ring detachment or straightforward advection.

Many models have been developed with respect to which these questions can be posed. Bower[3] and Samelson[26] studied kinematic models based on the meander structure of the Gulf Stream evident from spaghetti plots, such as shown in Figure 1. More recently, dynamically consistent models were formulated by del-Castillo-Negrete and Morrison[6] and Pratt, Lozier and Beliakova[21]. The first group used the Bickley jet (sech^{2}y profile) as the base flow coupled with superimposed neutral modes. Pratt et al used the cusped jets derived from a 1½ layer model in the paper by Pratt and Stern[22]. These cusped jets have piecewise constant potential vorticity, and the center of the jet is characterized by a discontinuity in the potential vorticity. Since these cusped jets are linearly stable, it is reasonable to model perturbations in the full flow field by superimposing on the base flow selected neutral modes. It is assumed that two waves are used and the first is a larger perturbation than the second. The first neutral mode introduces a characteristic speed and the steering lines occur where this matches the speed of the fluid particles in the base jet. As pointed out by both

Figure 10.

Adding a second neutral mode with a speed slightly greater than the first mode results in significant mixing across the region of the steering line. This is evident from the strong breakup of the stable (blue) and unstable (red) manifolds of the associated Poincare map. Again the intermingling is shown by the color coding, see Figure 7.
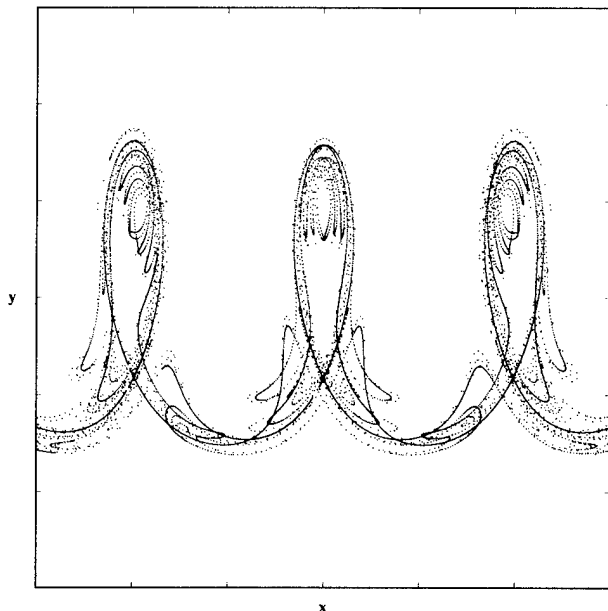
groups, in the regions near the steering lines chaotic trajectories can appear and, more importantly, advective mixing be facilitated. Such chaotic structures will be expected to appear when a second wave is superimposed on the flow field. If its wavenumber and frequency are unmatched to those of the primary wave, the resulting forcing on the velocity field is time dependent and such a scenario is known to produce chaotic motion.

A comment about potential vorticity is in order here, see the book by Pedlosky[19] for the relevant definitions and discussion. As observed recently in the paper by Brown and Samelson[5], a two-dimensional incompressible flow with time-periodic forcing, which preserves potential vorticity, cannot be chaotic if the gradients of the potential vorticity and the streamfunction are independent. Indeed, the Lagrangian trajectories are constrained in this case to 2-dimensional surfaces, determined by the potential vorticity contours, and will thus not be chaotic. As commented by del-Castillo-Negrete and Morrison[6], this apparent contradiction is resolved by the fact that flows under consideration are not exactly potential vorticity conserving. However, from the mathematical viewpoint, this breaking of the potential vorticity conservation arises from the approximations made in implementing the

model. These approximations are made in assuming that the flow field is given as a base flow with two neutral modes added. The full nonlinear field, which is only modelled by this linear superposition, is potential vorticity conserving, but this may not hold for the flow field that is actually used. Moreover, potential vorticity can be broken by the numerical approximations made in calculating the Lagrangian trajectories. Of course, in the real ocean potential vorticity is not conserved and we do expect orbits heteroclinic to stagnation points to break up in such a way as to produce chaotic motion. It would be preferable, however, if this effect was modelled directly rather than as a by-product of the approximations made. In other words, we would hope to be able to produce these effects of chaotic mixing by producing models that more accurately reflect the actual ways in which potential vorticity is broken, rather than through less accurate ways of modelling systems in which it is conserved. Nevertheless, the presence of chaotic mixing is credible whenever such heteroclinic orbits appear and we believe that it is a significant mechanism.

The models under consideration are effectively two-dimensional, and the effects of vertical motion may be quite significant. It has been suggested that mixing across a jet may occur more readily at deeper levels, see Lozier and Riser[13]. Combining this feature with the possibility of vertical motion offers some very tantalizing possibilities. The effects of depth can be studied within the stratified models discussed above as the depth does occur as a parameter within the flow field. Questions can then be asked about the dependence of advective mixing on depth, for instance: is mixing facilitated at lower depths? The picture one should keep in mind is that described by Pratt, Lozier and Beliakova[21] in which the base jet is bracketed by two steering lines determined by the primary wave. On the surface, these steering lines are well separated, but as one looks deeper, the steering lines move toward each other until they converge and cancel each other, at a certain depth. Below that depth the fluid particles of the base jet all move slower than the primary wave.

To study the dynamics of the Lagrangian trajectories in the vicinity of steering lines we began with the analytical model for a cusped jet velocity profile formulated by Pratt, Lozier and Beliakova[21]. The flow is taken to be two dimensional and is governed by a streamfunction $\psi(x,y,t)$. The Lagrangian particle motions satisfy the equation

$$\frac{dx}{dt} = -\frac{\partial \psi}{\partial y}$$

$$\frac{dy}{dt} = \frac{\partial \psi}{\partial x}$$

The base flow of the jet is a shear flow with velocity profile

$$U(y) = e^{-|y|}.$$

$$\psi_a(x,y,t) = a\Phi(y) \cos k(x - ct),$$

where the eigenfunction $\Phi(y)$ is given by

$$\Phi(y) = e^{-\kappa|y|}.$$

The wavenumber k, the wave speed c, and the cross-stream decay rate κ are related by

$$\kappa = \sqrt{1 + k^2}, \qquad c + 1 - \kappa^{-1}.$$

In a frame moving with speed c, the Lagrangian trajectories are solutions of the equations

$$\frac{d\zeta}{dt} = U(y) - c - a\,\Phi'(y) \cos k\zeta,$$

$$\frac{dy}{dt} = -a\,k\,\Phi(y) \sin k\zeta,$$ (6)

where we have introduced the variable $\zeta = x - ct$. As shown in [21], this system will have two steering lines, for appropriate values of c, and the structure of the trajectories near these lines will be of a row of cat's eyes, familiar from the Stuart vortex flow, see Figure 6. Increasing the speed c of the superimposed wave draws the steering lines closer to the centerline of the jet. The exponential form of $\Phi(y)$ introduces asymmetry into the shape of the periodic orbits and the meandering shape of the jet is more pronounced, as seen in Figure 7.

The break-up of these heteroclinic trajectories is forced by a second neutral wave being superimposed on the stream-function. This secondary wave is of the same form as the first wave,

$$\psi_2(x,y,t) = \varepsilon\Phi_2(y) \cos k_2(x - c_2t),$$

but the wave speed c_2 is chosen different from the speed c of the first mode. The wavenumber k_2 and speed c_2 are related as in (5), and the amplitude ε is taken to be small relative to a. The Lagrangian trajectories are now governed by a time-dependent vector field where the order ε time dependency is periodic with angular frequency $\omega = k_2(c_2-c)$. The vector field is of the form

$$\frac{d\zeta}{dt} = U(y) - c - a\Phi'(y) \cos k\zeta - \varepsilon\Phi'_2(y) \cos(k_2\zeta - \omega t),$$ (7)

$$\frac{dy}{dt} = -a\,k\,\Phi(y) \sin k\,\zeta - \varepsilon\,k\,\Phi_2(y) \sin(k_2\zeta - \omega t).$$

Since (7) is a time-dependent Hamiltonian system for ε 0, the secondary wave is expected to break the heteroclinic

orbits on either side of each set of cat's eyes. This can be verified by calculating the Melnikov function associated with the problem. This function gives the leading order term in the signed distance between the stable and unstable manifolds of two unstable periodic solutions which are created by the perturbation in the vicinities of the two unperturbed stagnation points. For the vector field (7) the Melnikov function can be written in the form

$$M(t_o) = \int_{-\infty}^{\infty} \{\psi_0 + \psi_a, \psi_2\}_{x = x^h(t-t_0)} dt,$$ (8)

where $x^h(t-t_0)$ is the unperturbed heteroclinic orbit connecting the stagnation points for $\varepsilon = 0$, and $\{.,.\}$ denotes the Poisson bracket in the ζ and y variables. The explicit form of $x^h(t-t_0)$ seems hopeless to determine, but it is in fact not needed for finding zeros of the Melnikov function. It turns out that, using the symmetry of $x^h(t-t_0)$ with respect to the fixed ζ line through the center of the unperturbed problem, one can argue that $M(t_0)$ admits isolated zeros. A similar reasoning yields that these zeros are transverse, therefore the heteroclinic connection between the unperturbed stagnation points breaks up, but individual transverse heteroclinic solutions between nearby unstable periodic motions survive.

This break-up can be observed numerically through the distinctive looping caused by transverse intersections and the associated heteroclinic tangle. Figure 8 shows the result of perturbing the flow shown in Figure 7 for the case when the wavenumber k_2 of the secondary mode is twice the wavenumber of the first neutral mode. An interesting feature here is that it is significantly harder to detect the presence of transverse intersections along the outside edge of the jet. This is similar to a feature noted by Samelson[26] for the kinematic meander model. The interesctions on the outer edge seem to occur at a much higher order, and it appears that the outside heteroclinics do not break at all. Whereas, when the steering lines draw closer to one another, the heteroclinics in the interior of the jet are easily detected. In agreement with the analysis for the derivative of the Melnikov function, we have observed numerically that the strong heteroclinic breakup can be made to occur on the opposite side of the loop by reversing the sign of the angular frequency ω. This implies that the regions of significant mixing may depend on the relative speeds of the two superimposed neutral waves, since the sign of ω depends on the difference of the wave speeds c and c_2. In particular, if the secondary mode is faster than the primary neutral mode, then the resulting mixing is more intense within the body of the jet, whereas the boundary of the body of the jet, viewed as being the two steering lines, is virtually intact. As a result, fluids particles are kept outside of the jet by the outer stable and unstable manifolds which form barriers to mixing. At the same time, if the wave speed of the secondary mode is smaller than that of the primary mode, this boundary breaks up and

being the two steering lines, is virtually intact. As a result, fluids particles are kept outside of the jet by the outer stable and unstable manifolds which form barriers to mixing. At the same time, if the wave speed of the secondary mode is smaller than that of the primary mode, this boundary breaks up and Lagrangian particle motions can penetrate into the jet via chaotic mixing. However, even in this second case the inside of the jet is bounded by the virtually unbroken inner separatrices and serves as a barrier to transport through the core of the jet.

As steering lines approach each other, which occurs as one goes deeper below the surface, it appears that mixing, both within and across the jet, should be facilitated. Our group is studying this in the context of the cusped jets. For the jet with a single cusp, the steering lines approach each other, but the limit is quite degenerate as they will converge exactly at the cusp. The jet clearly becomes very thin, but indications are that it remains a barrier, as seen in Figure 8.

In the Bickley jet case, [6] the phenomenon of separatrix reconnection occurs. In this scenario, heteroclinic orbits exist that stretch across the jet between the two rows of cat's eyes that lie either side of the jet centerline. This would appear to be a level at which mixing is strongly facilitated and can be realized across the entire jet. However, as pointed out by Pratt (private communication) this may be hard to realize in an actual situation because of the strong potential vorticity gradients. Indeed, this is corroborated by the single cusped jet case.

The phenomenon of convergent steering lines can also be studied in the context of the double cusped jet of Pratt et al.[2]. Here they will converge as the speed of the primary wave is reduced to match the speed at the center of the jet, which lies in a third region of constant potential vorticity between the two outer regions. In the case of a smooth jet profile, the derivative $U'(y)$ is necessarily zero at the speed at which the two steering lines converge. We have performed a local analysis to study the possible dynamics in such a situation. For simplicity, we assume that the converging steering lines occur at y=0 and that both $\phi(y)$ and $\Phi'(y)$ are non-zero at y=0. We introduce the following change of variables:

$$\zeta = x - ct, \quad \eta = a^{-\frac{1}{3}}y, \quad \tau = a^{\frac{2}{3}}t.$$

Retaining just the leading order terms of the vector field results in the following scaled equations,

$$\frac{d\zeta}{dt} = \frac{1}{2}U''(0)y^2 - a^{\frac{1}{3}}\Phi'(0)\cos k\zeta,$$

$$\tag{9}$$

$$\frac{d\eta}{dt} = -k\Phi(0)\sin k\zeta - \varepsilon a^{-1}k_2\Phi_2(0)\sin(k_2\zeta - a^{-\frac{2}{3}}\omega\tau).$$

At $\varepsilon = 0$ there are homoclinic loops separated by a distance $k\zeta = 2\pi$, and heteroclinic orbits form separatrices on only one

side of the jet. Figure 9 shows the resulting flow with one neutral mode superimposed and the parameters set to $U''(0)=2$, $\Phi(0)=1$, $\Phi'(0)=1$, and a= 0.01. A significant issue is whether the break-up of heteroclinics on the outside of the jet still occurs. By using the Melnikov function from (8), we have been able to show that it will occur in a uniform manner all the way down to the convergent steering line point. This indicates that the region of the convergent steering line presents no more of an effective barrier than at higher depths.

In the numerical simulation, when a second neutral mode is added to the streamfunction i.e., $\varepsilon > 0$ is set in (9), both the heteroclinic and homoclinic tangles are easily observed, as seen in Figure 10. The characteristic shape of the heteroclinic tangle is easily observable in the figure and it shows that the break-up of the heteroclinic orbit results in significant mixing. Further numerical experiments also indicate that particles do indeed traverse the entire width of the jet. More intricate calculations and additional numerical experiments are needed to ascertain whether it is a region of more efficacious mixing. Of particular significance are simulations for somewhat larger amplitudes of the secondary mode, as the dynamics in that case is not amenable to perturbation methods like the Melnikov method. Related results for two-dimensional maps suggest that for such larger perturbations most barriers to transport are destroyed and new mixing mechanisms are created.

Acknowledgements

Biographies

Christopher Jones is Professor of Applied Mathematics at Brown University. He received his Ph.D from the University of Wisconsin-Madison. He has held positions at the Universities of Arizona and Maryland before coming to Brown in 1990. His research interests include the applications of dynamical systems and the study of nonlinear waves. George Haller received his Ph.D. from California Institute of Technology. After a postdoctoral appointment at the Courant Institute of New York University, he joined the faculty of Brown in 1994. His research interests include dynamical systems applied to

fluid and analytical mechanics. Patrick Miller received his Ph.D. from the University of Massachusetts in 1994 and currently holds a postdoctoral appointment at Brown where he is working on the application of dynamical systems problems to oceanography. Jonathan Rubin is a graduate student at Brown working under the supervision of Christopher Jones.

References

1. V.I.Arnold, *Mathematical Methods of Classical Mechanics*, Springer-Verlag, NY, 1978.

2. R.P.Behringer, S.D.Meyers & H.L.Swinney, Chaos and mixing in geostrophic flows, *Physics of Fluids* A 3 (1991) 1243-1249.

3. A.S.Bower, A simple kinetic mechanism for mixing fluid parcels across a meandering jet, *Journal of Physical Oceanography* 19 (1991) 174-180.

4. A.S.Bower & T.Rossby, Evidence of cross-frontal exchange processes in the Gulf Stream based on isopycnal RAFOS float data, *Journal of Physical Oceanography* 19 (1989) 1177-1190.

5. M.G.Brown & R.M.Samelson, Particle motion in vorticity-conserving, two-dimensional incompressible flows, *Physics of Fluids* 6 (1994) 2875-2876.

6. D. del-Castillo-Negrete & P.Morrison, Chaotic transport by Rossby waves in shear flow, *Physics of Fluids* A 5 (1993) 948-965.

7. N.Fenichel, Persistence and smoothness of invariant manifolds, *Indiana Univ. Math. J.* 21 (1971), 193-226.

8. N.Fenichel, Geometric singular perturbation theory for ordinary differential equations, *J. Diff. Eqn.* 31 (1979), 53-98.

9. G.R.Flierl, V.D.Larichev, J.C.McWilliams & G.M.Reznik, The dynamics of baroclinic and barotropic solitary eddies, *Dyn. Atmos. Oceans* 5 (1980) 1-41.

10. J.Guckenheimer & P.Holmes, *Nonlinear Oscillations, Dynamical Systems, and Bifurcations of Vector Fields*, Springer-Verlag, NY, 1983.

11. C.Jones, M.Maxey & J.Rubin, Settling and asymptotic motion of aerosol particles in a cellular flow field, preprint (1994).

12. C.Jones, Geometric singular perturbation theory, in *C.I.M.E. Lectures, Session on Dynamical Systems*, in press.

13. M.S.Lozier & S.C.Riser, Potential vorticity sources and sinks in a quasigeostrophic ocean: beyond western boundary currents, *Journal of Physical Oceanography* 20 (1990) 1608-1627.

14. M.R.Maxey, The motion of small spherical particles in a cellular flow field, *Phys. Fluids* 30 (1987), 1915-1928.

15. M.R.Maxey & S.Corrsin, Gravitational settling of aerosol particles in randomly oriented cellular flow fields, *J. Atmos. Sci.* 43 (1986), 1112-1134.

16. R.P.Mied, A.D.Kirwan, Jr. & G.J.Lindemann, Rotating modons over isolated topography, *Journal of Physical Oceanography* 22 (1992) 1569-1582.

17. M.A.Kennelly, R.H.Evans & T.M.Joyce, "Small-scale cyclones on the periphery of a Gulf Stream warm core ring" *Journal of Geophysical Research* 90 (1985) 8845-8857.

18. A.D.Kirwan, Jr., R.P.Mied & B.L.Lipphardt, Jr., Rotating modons over isolated topography in a stratified ocean, preprint (1994)

19. J.Pedlosky, *Geophysical Fluid Dynamics*, Springer-Verlag, New York, 1979.

20. L.J.Pratt, J.Earles, P.Cornillon & J.-F.Cayula, The nonlinear behavior of varicose disturbances in a simple model of the Gulf Stream, *Deep Sea Research* 32 (1991) 591-622.

21. L.J.Pratt, M.S.Lozier & N.Beliakova, Parcel trajectories in quasigeostrophic jets part 1: neutral modes, to appear in *Journal of Physical Oceanography* (1995)

22. L.J.Pratt & M.E.Stern, Dynamics of potential vorticity fronts and eddy detachment, *Journal of Physical Oceanography* 16 (1986) 1101-1120.

23. H.Ridderinkhof & J.T.F.Zimmerman, Chaotic stirring in a tidal system, *Science* 258 (1992) 1107-1111.

24. V.Rom-Kedar & S.Wiggins, Transport in two-dimensional maps, *Arch. Rat. Mech. Anal.* 109 (1990) 239-298.

25. V.Rom-Kedar, Homoclinic tangles-classification and applications, *Nonlinearity* 7 (1994) 441-473.

26. R.M.Samelson, Fluid exchange across a meandering jet, *Journal of Physical Oceanography* 22 (1992) 431-440.

27. H.Stommel, Trajectories of small bodies sinking slowly through convection cells, *J. Mar. Res.* 8 (1949), 24-29.

28. K.K.Tio, A.Linan, J.C.Lasheras & A.M.Ganan-Calvo, On the dynamics of buoyant and heavy particles in a periodic Stuart vortex flow, *J. Fluid Mech.* 254 (1993) 671-699.

29. M.Visser, On the transport of fine marine sediment in the Netherlands coastal zone, University of Utrecht, The Netherlands, 1993.

30. S.Wiggins, *Introduction to Applied Nonlinear Dynamical Systems and Chaos*, Springer-Verlag, NY, 1990.

31. S.Wiggins, *Chaotic Transport in Dynamical Systems*, Springer-Verlag, NY, 1992.

32. J.A.Yoder, S.G.Ackleson, R.T.Barber, P.Flament & W.M.Balch, A line in the sea, *Nature* 371 (1994), 689-692.

Planforms at the Onset of Instability in Double Diffusive Convection

Yuriko Yamamuro Renardy
Department of Mathematics
Virginia Polytechnic Institute and State University

Introduction

The subject of double-diffusive convection covers the study of fluids in which there are gradients of two or more properties with different molecular diffusivities. Many interesting phenomena have been discovered in the context of the ocean, where heat and salt provide the competing properties and hence this subject is also known as thermohaline or thermosolutal convection. An overview of the area is given in the recent articles by Schmitt (1994, 1995). The following paragraph takes snippets from them in order to give a quick glimpse of the history.

Over a century before Melvin Stern discovered salt fingers, W. Stanley Jevons performed the first salt finger experiment in an attempt to model cirrus clouds. Remarkably, he seemed to realize that a more rapid diffusion of heat relative to solute played a role in the experiments. However, he over-simplified the physics and incorrectly assumed that the "interfiltration of minute, thread-like streams" was a general result of superposing heavy fluid over light fluid. Interestingly, Lord Rayleigh became aware of these experiments more than two decades later. He repeated the Jevons' experiments at the Cavendish Laboratory in Cambridge in April, 1880. The results led him to initiate the study of buoyancy effects in fluids by formulating several stability problems for a stratified, but non-diffusive fluid. His neglect of diffusion meant that he

missed an opportunity to discover double-diffusive convection. The modern study of double-diffusive convection began with Melvin Stern's article on "The Salt Fountain and Thermohaline Convection" in 1960. Stommel et al (1956) had suggested that a flow (the salt fountain) would be driven in a thermally-conducting pipe, but it was Stern who realized that the two order of magnitude difference in heat and salt diffusivities allowed the ocean to form its own pipes. These later came to be known as "salt fingers". Stern also identified the potential for the oscillatory instability when cold, fresh water overlies warm, salty water in the 1960 paper. This "diffusive-convection" process was demonstrated later by Turner and Stommel (1964).

For the purpose of this article, we will focus on the situation with warm salty fluid below cold fluid. The fluid lies between two horizontal walls placed a distance L apart, and is of infinite extent in the horizontal (x-y) plane. The warm fluid tends to rise and the salty fluid, being heavier than fresh fluid, tends to fall, so that if we begin with the liquid at rest, then increasing the temperature difference will eventually destabilize the rest state and yield either an oscillatory motion or a steady convective motion. In particular, we will address the oscillatory onset of instability (the "diffusive-convection" problem) and examine a family of patterns that may arise. We wish to find new solutions that bifurcate from the rest state, and determine their stability to perturbations.

Methodology

Stability of Fluid Motions

We begin by identifying the velocity, pressure, temperature and solute concentration that satisfy the governing equations and which represent a "base flow". The velocity field for the base flow that we will investigate in the double diffusion problem is zero (the "rest state"), the temperature and solute concentrations depend linearly on the vertical variable z, and the pressure field is a quadratic polynomial in z. If this base flow is disturbed slightly, then the disturbance may decay, or may grow, depending on whether the flow is stable or unstable. If the flow is unstable, then the solution will change from the base flow to something else, but to what? We will give a partial answer by considering small disturbances, and how the disturbances that grow the fastest interact with each other at the conditions close to the onset of instability (the "critical situation"). We therefore express the total solution as a superposition of the base flow and a perturbation, and write down the equations that govern the perturbation. In the following, a solution will usually mean a solution for the perturbation.

Spatial Periodicity

The governing equations for the perturbation to the base flow show that if one stands at the origin and looks in any direction, the problem looks the same. Many bifurcation problems in fluid mechanics involve one or more spatially unbounded directions and a continuum of modes. A full description of the set of bifurcating solutions in such a context is a rather formidable problem that has not been solved. Therefore, one typically imposes some spatial periodicity on the problem and then confines attention to solutions satisfying this given periodicity. For instance, one may look for solutions that are periodic with respect to the vectors

$$x_1 = W \cdot (\frac{\sqrt{3}}{2},\frac{1}{2},0), \quad \text{and} \quad x_2 = W \cdot (0,1,0).$$

These vectors are said to span a hexagonal lattice of period W. In the x and y directions, the solution is then doubly periodic; that is, at any time t, the temperature at the position $x = (x,y,z)$ is equal to the value at $x+n_1\ x_1+n_2\ x_2$, for any integer n_1, n_2. The lattice obtained from this double periodicity is invariant under the symmetries of the hexagon;that is, rotation by multiples of 60 degrees, reflection across the vectors a_i defined by

$$a_1 = \frac{4\pi}{W\sqrt{3}} (1,0,0), a_2 = \frac{4\pi}{W\sqrt{3}} (-\frac{1}{2}, \frac{\sqrt{3}}{2},0), a_3 = -a_1 - A_2, \quad (1)$$

and reflection across axes perpendicular to the a_i.

The same periodicity condition holds for the other unknowns: the solute concentration, velocity field and pressure field. This simplifies the problem immensely and allows us to use a Fourier series expansion of the solution. We next describe a method that can be applied to find ordinary differential equations for the dominant Fourier amplitudes, and thereby find families of spatially-periodic structures on a planar lattice. Rolls and hexagons are two of the solutions that are periodic on a hexagonal lattice, and often observed in convection problems. Other lattices that may be considered are the square and rhombus (Golubitsky, Swift and Knobloch, 1984; Dionne, Golubitsky, Silber and Stewart, 1994).

Center Manifold Theory and Dynamical Systems

The analysis of spatially periodic bifurcating solutions and their stability proceeds in two steps. First, the governing equations are reduced by projections to a finite number of nonlinear ordinary differential equations (Iooss and Joseph, 1980, Chow and Hale, 1982). These are evolution equations. The center manifold theorem is invoked for this purpose. Roughly speaking, the theorem says that in the neighborhood of criticality, the dynamics is governed by the interactions among the finitely many critical modes. This places the problem in the framework of dynamical systems. At this stage, much of the details of the original partial differential equations and boundary conditions now appear in the coefficients of the evolution equations. Thus, seemingly different physical prob-

Figure 1.

The neutral stability curve for the oscillatory onset (line) and steady onset (dashed line) of instability for the stress-free problem is shown. The Lewis number is $\tau < 1$.
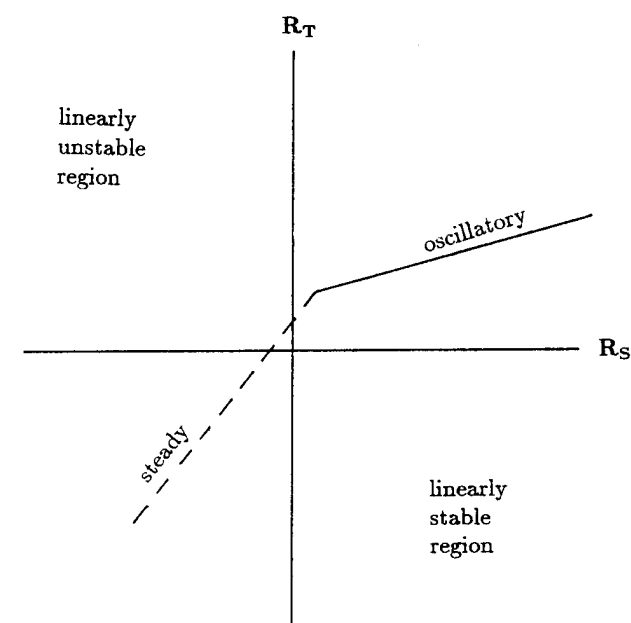
Figure 2.

We display the four standing wave solutions: standing rolls, standing hexagons, standing regular triangles, and standing patchwork quilt. These are contour plots for an amplitude function, e.g., the vertical component of the velocity. (Photographs for these figures were taken by Prof. David Wagner, Department of Mathematics, University of Houston, Texas.)

Standing Rolls

Standng Hexagons

Standing Regular Triangles

Standing Patchwork Quilt
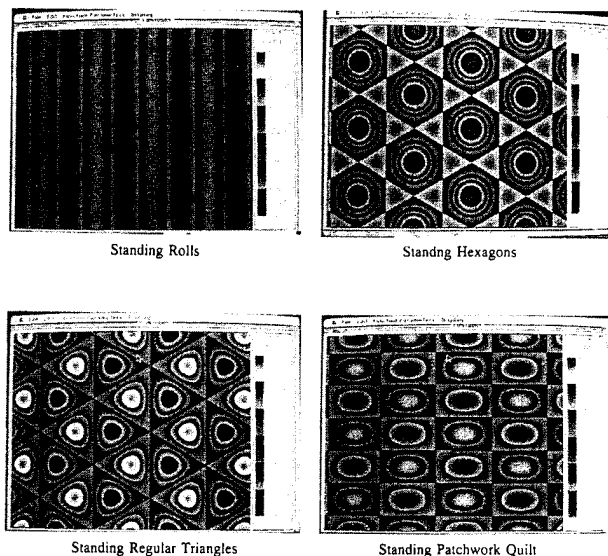
lems will be seen to reduce to the same types of evolution equations. Secondly, the existence and stability of the bifurcating solutions are determined by analyzing the system of ordinary differential equations. This general methodology handles a large class of stability problems, where the onset of instability is due to just a finite number of modes with the rest of the modes being stable, as is typical for viscous flows.

Governing Equations

A fluid is assumed to lie between two walls placed at z^* = 0 and $z^* = L$ in the (x^*, y^*, z^*) plane. Asterisks denote dimensional variables. The upper plate is kept at a constant temperature θ^*_0 with solute concentration S^*_0, and the lower boundary is kept at a higher temperature θ^*_1 and a higher solute concentration S^*_1; $\theta^*_0 < \theta^*_1, S^*_0 < S_1^*$. At temperature θ^*_0, the fluid has thermal coefficient of volume expansion $\hat{\alpha}$, solute coefficient of volume expansion $\hat{\beta}$, thermal diffusivity κ_T, solute diffusivity κ_S, viscosity μ, density ρ_0, and kinematic viscosity $v=\mu/\rho_0$.

Dimensionless variables (without asterisks) are as follows: $(x, y, z) = (x^*, y^*, z^*) / L$, $t = \kappa_T t^*/L^2$, $v = v^* L/\kappa_T$, $\theta = (\theta^*-\theta^*_0)/(\theta^*_1-\theta^*_0)$, $S= (S^*-S^*_0)/(S^*_1-S^*_0)$, $p = p^* L^2/(\rho_0\kappa^2_T)$.

A thermal Rayleigh number R_T, a salinity Rayleigh number R_S, a Prandtl number P, and Lewis number τ are defined by:

$$R_T = g\hat{\alpha}\,(\theta^*_1 - \theta^*_0)\, L^3/(\kappa_T v), \quad R_S = g\,\hat{\beta}\,(S^*_1 - S^*_0)\, L^3/(\kappa_T v),$$

$$P = v/\kappa_T, \quad \tau = \kappa_S/\kappa_T.$$

where g denotes gravitational acceleration, and a dimensionless measure of gravity is $G=gL^3/k_T^2$.

A basic solution is

$$v = 0, \quad \theta = 1-z, \quad S = 1-z, \quad p = p_0 - Gz + (R_T - R_S)\,P\,(z - \frac{z^2}{2}),$$

where p_0 is a constant. Since we are concerned with the stability of this rest state and with solutions bifurcating from it, we set up the problem for the perturbations $\theta, S, \tilde{p}$ and $v =$ (u, v, w) to this solution. The equations satisfied by these variables are:

the transport equations for the temperature and solute concentration

$$\dot{\theta} - w - \Delta\theta = - (v \cdot \nabla)\,\theta, \tag{2}$$

$$\dot{S} - w - \tau\Delta S = - (v \cdot \nabla)\,S, \tag{3}$$

the Navier-Stokes equation with the Oberbeck-Boussinesq approximation

$$\dot{v} - P \Delta v + \nabla\tilde{p} + (R_S PS - R_T P\theta)\,e_z = - (v \cdot \nabla)\,v, \tag{4}$$

and incompressibility

$$\text{div } v = 0. \tag{5}$$

Values for the temperature and solute concentration are prescribed at the walls:

$$\theta = 0, \quad S = 0, \quad \text{at} \quad z = 0 \quad \text{and} \quad z = 1. \tag{6}$$

The velocity boundary condition at the walls is the "no-slip" condition:

$$v = 0, \quad at \quad z = 0 \text{ and } z = 1. \tag{7}$$

Alternatively, one may use the "stress-free" boundary condition (zero normal velocity and zero shear stress):

$$w = 0, \frac{\partial u}{\partial z} + \frac{\partial w}{\partial x} = 0, \frac{\partial v}{\partial z} + \frac{\partial w}{\partial y} = 0, \quad at \quad z = 0,1. \tag{8}$$

For the stress-free problem, the eigenfunctions are available in closed form in terms of trigonometric functions (Baines and Gill, 1969, Huppert and Moore, 1976, Turner, 1979, Nagata and Thomas, 1984, Knobloch, 1985, Deane et al, 1987, Knobloch et al, 1986), and therefore the weakly nonlinear

We display the three travelling wave solutions. The upper pattern shows travelling rolls. The lower patterns are the travelling patchwork quilt (1) and the travelling patchwork quilt (2). The arrows indicate the direction of travel. (photographs by David Wagner)

k_1

Travelling Rolls

k_2

Travelling Patchwork Quilt (1)

$k_1 . k_3$

Travelling Patchwork Quilt (2)
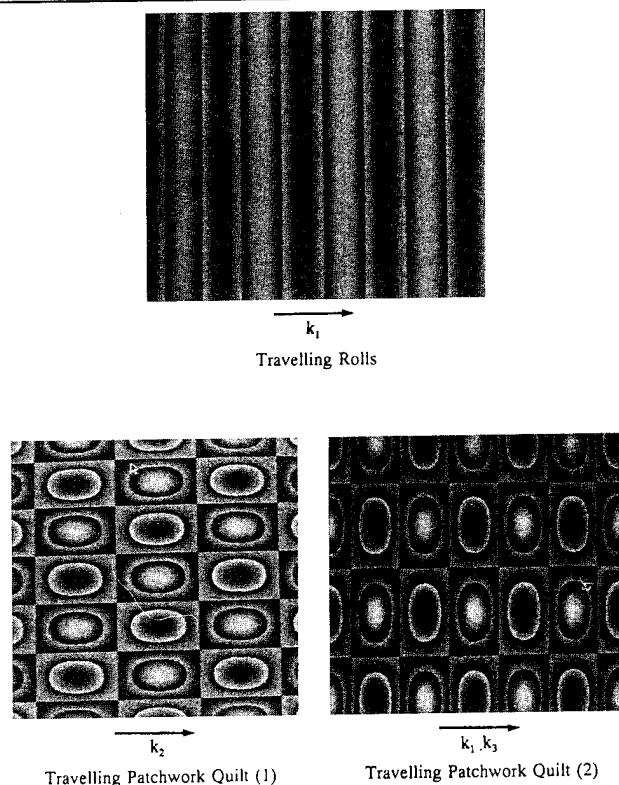
analysis can be done explicitly. This explicit representation is not available for the case of no slip, and a computational approach is then used for the analysis. The answer to the question of which type of velocity boundary condition is pertinent, lies in which phenomenon one is trying to describe. The use of the stress-free condition is relevant for modeling situations where the fluid layer is not bounded by walls but by free surfaces; for example, double diffusive actions may be taking place in a sandwiched layer at some depth say, in the ocean.

The set of unknowns, $v, \tilde{p}, \tilde{S}$ and θ and θ, is denoted by Φ. Equations (2) - (8) can be written in the schematic form

$$L\Phi = N_2 (\Phi, \Phi),$$

Here the operator L incorporates the linear terms, while N_2 stands for the quadratic terms.

Linear Stability Analysis

For the case of infinitesimally small perturbations, we linearize (9). The rotational symmetry of the problem about the vertical axis shows that we can ignore the y dependence

and pose the linearized problem in the x-z plane. The method of separation of variables is used to express the solutions as $\exp(i\alpha x + \sigma t)$ multiplied by a function of z. The real linear operator L has the form $A + \frac{d}{dt} B$, so that we are seeking eigenfunctions ζ which satisfy $(A + \sigma B)\zeta = 0$. The wavenumber of the perturbation is α and the growth rate is Re σ. We wish to map out the regions of stability (Re $\sigma < 0$) and instability, by locating the neutral stability curve (Re $\sigma = 0$).

Figure 1 shows the neutral stability curve for the stress-free problem (Nield, 1967, Baines and Gill, 1969) for the case $\tau < 1$, which is typical for many applications, including the ocean media. The neutral stability curve consists of two lines meeting at a Takens-Bogdanov point. The steady onset (dashed line) is along

$$R_T = \frac{R_S}{\tau} + \frac{27\pi^4}{4},$$

and the oscillatory onset is along

$$R_T = \left(\frac{P+\tau}{P+1}\right) R_S + (1+\tau)(1+\frac{\tau}{P}) \frac{27\pi^4}{4}$$

The critical wavenumber is $\alpha = \pi / \sqrt{2}$, the same along the entire neutral stability curve.

For the no slip problem, the onset conditions need to be computed numerically. For our numerical results, we use the Chebyshev-tau method, which approximates the eigenvalues σ with infinite-order accuracy. This is a spectral method (Orszag, 1971, Gottlieb and Orszag, 1983) in which the z-dependence of the eigenfunctions is expressed in terms of Chebyshev polynomials. In this manner, the linear stability problem is discretized into a matrix eigenvalue problem. The neutral stability curve for the steady onset is

$$R_T = \frac{R_S}{\tau} + 1707.765, \qquad \alpha = 3.12.$$

The neutral stability curve for the oscillatory onset is more complicated. This curve lies above that of figure 1, in that the critical thermal Rayleigh number is higher at each R_S. Moreover, the critical wavenumber increases with R_S.

Nonlinear Analysis

Background

In the two-dimensional case, there is a critical eigenfunction representing waves traveling to the right (with wavenumber α) and there is another one traveling to the left (with wavenumber $-\alpha$). These interact nonlinearly to produce traveling and standing wave solutions. In this situation, if both the standing and traveling waves bifurcate supercritically, then one of them is stable (Ruelle, 1973). Past work on nonlinear

We display the oscillating triangles. Upper patterns: t=0, t=T/24, T is the period. Middle patterns: t=T/12, t=T/8. Lower pattern: t=T/6. (photographs by David Wagner)

t=0

t=1/24

t=1/12

t=1/8

Oscillating Triangles

t=1/6
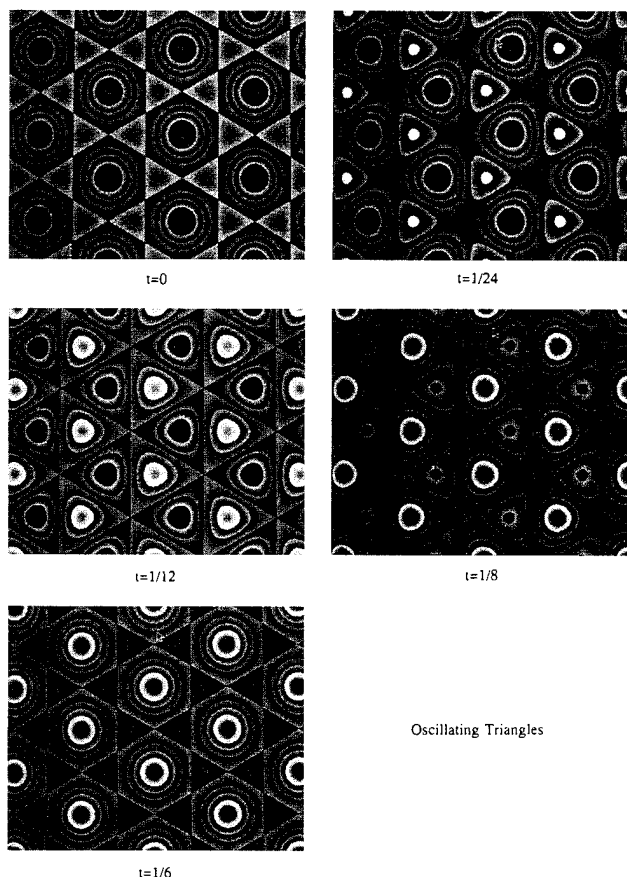
analysis has been on the stress-free problem (Knobloch, 1985). Deane et al (1987) derive the amplitude equations for the left- and right-traveling waves. At the least, they need to calculate up to third order in the amplitude functions. The calculation of the coefficients in the equation yields the Landau coefficient which determines whether the solution is supercritical or not. They find that the third-order Landau coefficient for the traveling wave turns out to be zero. This degeneracy appears to be a coincidental one (Knobloch et al, 1986) due to the adoption of the stress-free condition. The standing wave solution is supercritical, indeterminate and subcritical, respectively, for R_S less than, equal to and greater than 14585.4 for the case $\tau=10^{-1/2}$, $P = 1$. At the fifth order, Deane et al find that the traveling wave solution bifurcates supercritically, so that there is a range of R_S for which the traveling wave solution is stable.

What are the third order Landau coefficients, and what is the stable solution for the no slip case? Computations at the above values of Lewis and Prandtl numbers for $R_S=10^4$, 14585.4, and 10^5 reveal that the solutions are both unstable (Renardy, 1993). As expected, the selection mechanism is sensitive to the boundary conditions.

What other periodic solutions are there in the fully three-dimensional planform problem, and are they stable to the more general doubly periodic disturbances in the x-y plane? The two-dimensional solutions we have discussed correspond to standing rolls and traveling rolls in three dimensions. The three-dimensional stress-free problem has been studied by Nagata and Thomas (1984). For oscillatory onset, they present the linear stability of standing rolls, standing squares and standing hexagons to perturbations restricted to have the same symmetry as the solutions. For example, they examine whether hexagon pattern solutions are locally asymptotically stable with respect to hexagon pattern disturbances, and whether the roll solutions are stable with respect to roll-like disturbances. The next issue is the competition, say between rolls and hexagons, and the investigation of the traveling wave solutions.

Center Manifold Theorem and Dynamical Systems

The fluid properties are regarded as fixed and we define a bifurcation parameter $\lambda=R_T-R_{TC}$, where R_T is the thermal Rayleigh number and R_{TC} is its critical value. Solutions Φ with the periodicity of the hexagonal lattice are sought. Details of this calculation are found in Renardy (1993).

At criticality ($\lambda=0$), there is a pair of complex conjugate eigenvalues $\pm i\omega$ of the linearized problem, and each of them has six eigenfunctions. For λ near 0, $-\mu(\lambda)$ denotes the eigenvalue which arises from perturbing $-i\omega$. We denote by $\zeta_\kappa(\lambda)$, k=1,2,...,6 the eigenfunctions belonging to $-\mu(\lambda)$, i.e.

$$L\,(-\mu(\lambda))\zeta_k(\lambda) = 0,$$

and those belonging to $-\bar{\mu}(\lambda)$ are their complex conjugates. We will need to compute the eigenfunctions at $\lambda=0$.

The critical eigenfunction computed in the (x,z)-plane has the form $\zeta_1 = \zeta(z)\exp(ia_1 \cdot x)$, where $a_1=(\alpha,0,0)$, $x =(x,y,z)$, and α is the critical wavenumber. We may visualize the six eigenfunctions as follows. The vectors $\pm a_1$, $\pm a_2$ and $\pm a_3$ defined by equation (1) emanate from the center of a hexagon and terminate at its six vertices. The critical eigenfunctions are waves propagating in the directions of a_1, a_2, a_3 and $- a_1, - a_2$, $- a_3$. We denote the (complex) amplitude of the wave propagating in the direction of a_i by z_i and the amplitude of the wave propagating in the direction of $- a_i$ by z_{i+3}.

We can decompose a solution Φ in the form

$$\Phi = \Phi_1 + \Psi,$$

$$\Phi_1 = 2 \operatorname{Re} \sum_{k=1}^{6} z_k \, \zeta_k \,, \qquad (10)$$

where z_i are the complex-valued amplitude functions and Ψ represents a superposition of eigenvectors (and possibly generalized eigenvectors) belonging to stable eigenvalues. To use the Center Manifold Theorem, we need to have the fact that Ψ consists of stable modes. The expression on the right hand side of (10) converges to Φ in the mean square. The ζ_i and the functions in Ψ form a complete set. We wish to find equations that govern the evolution of the amplitude functions z_i. In order to do that, we need to find an explicit approximation to Ψ for small perturbations; at this stage, we invoke the Center Manifold Theorem.

The *Center Manifold Theorem* states that, in a neighborhood of $\Phi=0$, there is a manifold Γ (called the center manifold) of the form $\Psi=\tau(z_1,z_2,z_3,z_4,z_5,z_6)$ with the following properties:

1. All solutions with initial data on the center manifold remain on the center manifold as long as they remain small.

2. All small periodic solutions lie on the center manifold.

3. The stability of a small periodic solution is determined by its stability within the center manifold, in other words, all Floquet multipliers corresponding to directions outside the center manifold are stable.

These properties imply that only quadratic terms in the asymptotic approximation to the center manifold are required. Thus, the first property above is used to write the following expression

$$\Psi = \Psi_2 + ..., \qquad \Psi_2 = 2 \operatorname{Re} \left(\sum_{i,j=1}^{6} z_i \, z_j \, \psi_{ij} + z_i \, \bar{z}_j \, \chi_{ij} \right),$$

where the dots indicate terms of higher than quadratic order. The ψ_{ij} and χ_{ij} contribute to second harmonics and the mean flow mode.

The second property above says that the solutions of interest (the small periodic solutions, taking into account the nonlinear terms) are found on the center manifold. These are solutions close to the linear eigenfunctions. There need not be a center manifold if amplitudes become large.

By forming appropriate inner products and projections onto appropriate spaces, we are able to calculate the functions ψ_{ij} and χ_{ij}. The total solution Φ, accurate to second order, is now substituted back into the governing equations, leaving the z_i as the only unknowns. After further projections, using the symmetries of the hexagonal lattice and the theory of normal forms, the following reduced system is obtained:

Figure 5.

Wavy rolls (1). Top first row: t=0, t=T/16, T is a period. Second row patterns: t=T/8, t=3T/16. Third row: t=T/4, t=5T/16. Fourth row: t=3T/8, t=7T/16. Fifth row: t=T/2. (photographs by David Wagner)
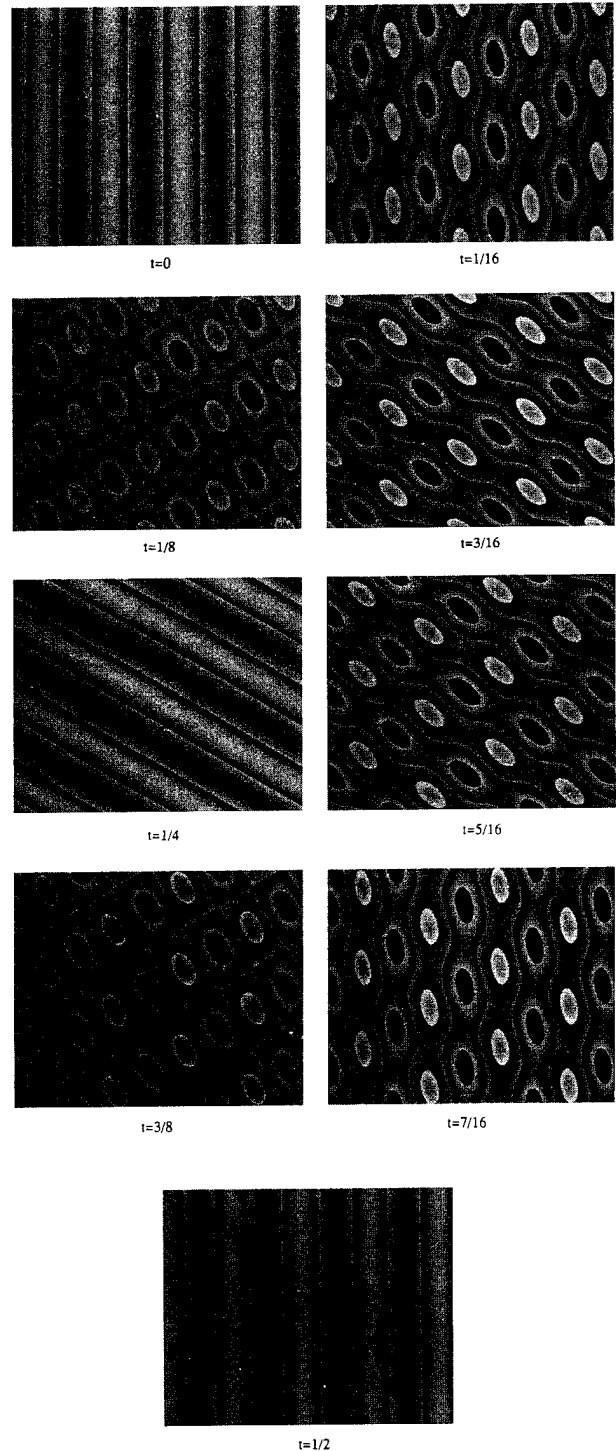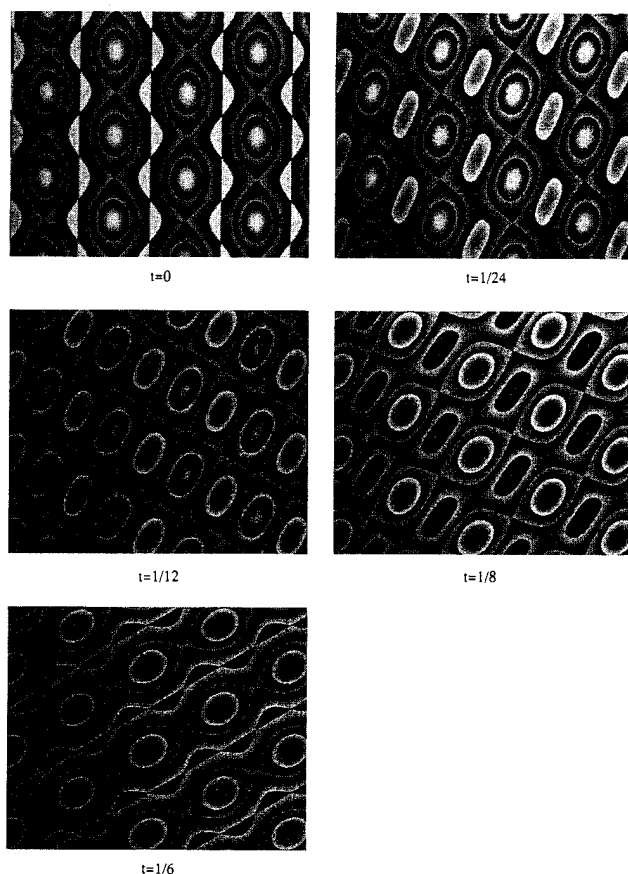
Figure 6.

Twisted patchwork quilt. Upper patterns: t=0, t=T/24, T is a period. Middle patterns: t=T/12, t=T/8. Lower pattern: t=T/6. (photographs by David Wagner)

t=0

t=1/24

t=1/12

t=1/8

t=1/6

$$\frac{dz_i}{dt} + F_i\,(z_1,z_2,z_3,z_4,z_5,z_6,\lambda) = 0, i = 1,\ldots,6, \qquad (11)$$

$$F_1\,(z_1,z_2,z_3,z_4,z_5,z_6,\lambda) = \mu\,(\lambda)\,z_1 + \alpha_1\,(\lambda)\,|\,z_1\,|^2\,z_1 + \alpha_2\,(\lambda)\,|\,z_4\,|^2\,z_1$$

$$+\alpha_3\,(\lambda)\,(\,|\,z_2\,|^2 + |\,z_3\,|^2)\,z_1 + \alpha_4\,(\lambda)$$

$$(\,|\,z_5\,|^2 + |\,z_6\,|^2)\,z_1 + \alpha_5\,(\lambda)\,(z_2\,z_5 + z_3\,z_6)\,\bar{z}_4 + \ldots$$

The dots denote terms of higher order, and $\alpha_1,\ldots,\alpha_5$ denote Landau coefficients. The F_i, i=2,...,6 are related to F_1 by properties of the hexagonal symmetry. We have now reduced the governing equations to a system of six complex nonlinear ordinary differential equations.

Pattern Selection on the Hexagonal Lattice

In (11), we set $u = (z_1,z_2,z_3,z_4,z_5,z_6)$, and obtain

$$\frac{du}{dt} + F\,(u,\lambda) = 0, \qquad (12)$$

where $u \in \mathbb{R}^{12}$ and λ is a real parameter. Starting with an equation of this general form, Roberts, Swift and Wagner (1986) use group theory to classify new solutions and determine their stability properties by considering their symmetries. This approach has allowed them to find a larger family of solutions than was previously available. Their results have a generality in that they apply to other problems that can be expressed in the form of (12) and have the same symmetries. They find eleven qualitatively different classes of bifurcated solutions: (i) Standing rolls, (ii) Standing hexagons, (iii) Standing regular triangles, (iv) Standing patchwork quilt, (v) Travelling rolls, (vi) Travelling patchwork quilt (1), which is always unstable, (vii) Travelling patchwork quilt (2), (viii) Oscillating triangles, (ix) Wavy rolls (1), (x) Twisted patchwork quilt, (xi) Wavy rolls (2). These are solutions which have enough symmetries so that the twelve degrees of freedom are reduced to two. For example, invariance under rotations by multiples of 60 degrees and reflections across the axes of the hexagon yields a two-dimensional solution set where the z_i are equal, called the standing hexagon. The conditions for stability of each solution with respect to perturbations with the double periodicity is also provided in Roberts et al. To apply these results to a specific problem, it is necessary to calculate the coefficients that appear in (11).

Figures 2 - 7 are contour plots of the vertical component of the velocity for each of the solutions. Solutions (i) - (iv) are standing waves, i.e., the patterns simply oscillate with time, and are shown in figure 2. These plots can be thought of as pictures taken at time zero. Solutions (v) - (vii) are traveling waves, i.e., the pattern moves to the right without changing its shape, and are shown in figure 3. The four remaining solutions, shown in figures 4 - 7, are neither standing nor traveling waves. The time dependence is indicated by a series of pictures. For example, figure 4 shows the oscillating triangle at t=0, 1/24, 1/12, 1/8 and 1/6 of a period. The pattern evolves through the rest of the period before going back to the t=0 picture.

Numerical Results for the Oscillatory Onset for Double Diffusion

For Lewis number $\tau=10^{-1/2}$ and Prandtl number $P = 1$, we have seen that traveling waves are stable in the two-dimensional stress-free problem for a range of solutal Rayleigh numbers R_S, while it is unstable for the no slip problem. We pursue the no slip problem as a model for the fluid bounded by walls, and examine the stability of the 11 solutions in the

three-dimensional case. To achieve an oscillatory onset, the solutal Rayleigh number should be larger than approximately 10^3; results in the range $10^3 \leq R_S \leq 10^6$ will be presented. It is found that the solutions are unstable until the solutal Rayleigh number becomes relatively large. As the R_S increases, so does the R_T at criticality, since the solute concentration effect must counteract the thermal effect to provide for the oscillatory onset (at $R_S = 2 \times 10^6$, the critical R_T is of order 1 million). For solutal Rayleigh numbers between 8×10^5 and 8.5×10^5, the standing rolls are stable and the other 10 solutions are unstable. There is a window of R_S from 9.0×10^5 to about 2.0×10^6, where all 11 solutions are unstable. For $R_S \approx 4.0 \times 10^6$, either the standing hexagons or the standing regular triangles is stable but not both, and the remaining 9 solutions are unstable. As a reminder of the scales involved, the typical properties for water (Drazin and Reid, 1981) are: $\hat{\alpha} \approx 5 \times 10^{-4} K^{-1}$, $\theta_1^* - \theta_0^* \leq 10$ K, $\kappa_T \approx 10^{-3}$ cm^2/sec, $v \approx 10^{-2}$ cm^2/sec, $g \approx 10^3$ cm/sec^2. Substituting these into the definition for the thermal Rayleigh number to be 1 million, we find $L^3 \approx 2$, L being measured in cm.

The heating of cold salty water is more appropriately modelled by a Prandtl number of $P = 10.0$ and Lewis number $\tau = 0.01$. Numerical results were obtained for solutal Rayleigh numbers up to order a million. At low Rayleigh numbers, the solutions were found to be unstable. For R_S between 10^6 to 10^7, the standing rolls are stable and the other solutions are unstable. For $R_S \approx 2 \times 10^7$, three of the standing wave solutions are found to be stable. These are the standing rolls, the standing patchwork quilt, and either the standing hexagons or the standing regular triangles. If this situation were realized in nature, we may see a coexistence of these solutions, a patch of one lying next to another.

We have obtained numerical results for two sets of Prandtl and Lewis numbers; the 11 solutions tend to be unstable for low Rayleigh numbers, while a number of standing wave solutions may be stable at higher Rayleigh numbers.

Outlook for the Future

The center manifold reduction method is applicable to onsets of instability, whether steady or oscillatory or both, in many different viscous flow situations, and continues to be applied to a variety of problems. The group theoretic approach for finding classes of solutions to the nonlinear ordinary differential equations by taking advantage of the symmetries in the problem is particularly useful for convection problems; recent examples include ferrofluids (Silber and Knobloch, 1991), viscoelastic liquids (Renardy and Renardy, 1992), interfacial stability in a two-layer system (Renardy and Renardy, 1988; Joseph and Renardy, 1993) and magnetoconvection (Clune and Knobloch, 1994). On the one hand, these analytical results serve to explain observed phenomena, and on the other, they encourage future search for these patterns in the labora-

tory. For instance, we have found that three different patterns can coexist in certain parameter ranges. It would be interesting to see which one(s) of these can be set up under experimental conditions.

This article has taken the oscillatory onset for the double diffusion problem and highlighted the dynamical systems approach coupled with group theory. Apart from the oscillatory onset, the double diffusion problem can have a steady onset or the case where the oscillatory onset merges into a steady onset. In particular, the case of the steady onset is relevant for the investigation of salt fingers. The subject of salt fingers, and their stability, is an ongoing area of research, where mathematical modeling together with the type of analysis presented here provide fertile grounds for future interdisciplinary collaboration. For instance, why are square patterns commonly observed (Proctor and Holyer, 1986)? and why are

Figure 7.

Wavy rolls (2). Upper patterns: t=0, t=T/24, T is a period. Middle patterns: t=T/12, t=T/8. Lower pattern: t=T/6. (photographs by David Wagner)

t=0

t=1/24

t=1/12

t=1/8

t=1/6
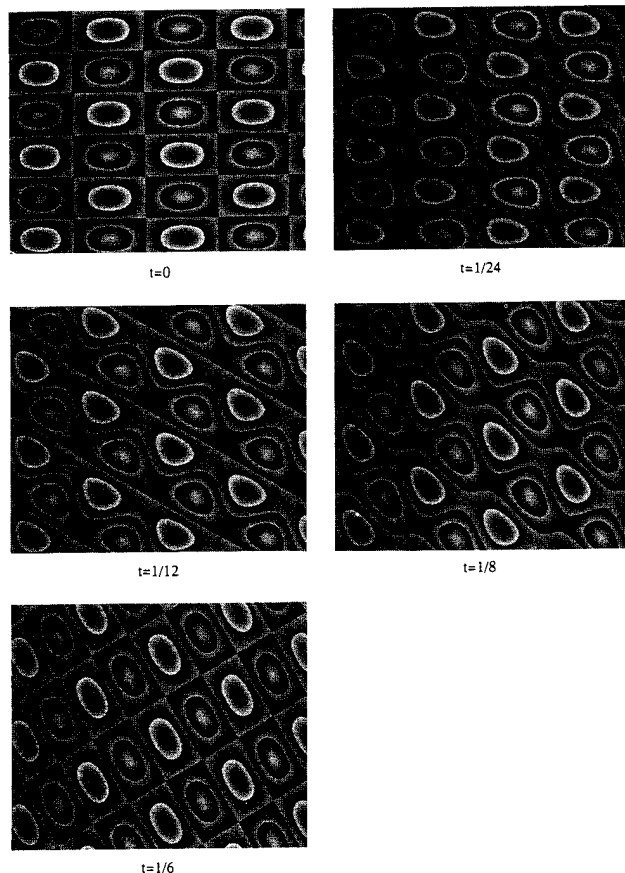
there triangular and asymmetric patterns in certain regions of the ocean (Schmitt, 1994b)?

Acknowledgements

Biography

Yuriko Yamamuro Renardy is a Professor of Mathematics at Virginia Polytechnic Institute and State University. She received her BSc (Hons.) from The Australian National University in 1977 and her PhD from The University of Western Australia in 1981. She spent the next five years in a variety of positions, as Research Associate and later Program Coordinator at the Mathematics Research Center, University of Wisconsin-Madison, and as instructor at the University of Minnesota. She joined the faculty at Virginia Polytechnic Institute and State University in 1986. Her major research interests are in hydrodynamic stability, convection, interfacial stability in multi-layer flows and viscoelastic flows.

References

1. P. G. Baines and A. E. Gill, J. Fluid Mech. 37 (2), 289 (1969)

2. S.-N. Chow and J. K. Hale, *Methods of Bifurcation Theory*, Springer Verlag (1982)

3. T. Clune and E. Knobloch, Physica D 74, 151 (1994)

4. A. E. Deane, E. Knobloch and J. Toomre, Phys. Rev. A 36 (6), 2862 (1987)

5. B. Dionne, M. Golubitsky, M. Silber and I. Stewart, Trans. Roy. Soc. Lond. Series A , in press (1994)

6. P. G. Drazin and W. H. Reid, *Hydrodynamic Stability*, Cambridge University Press (1981)

7. M. Golubitsky and I. Stewart, Arch. Rat. Mech. Anal. 87, 107 (1985)

8. M. Golubitsky, J. W. Swift and E. Knobloch, Physica 10D, 249 (1984)

9. D. Gottlieb and S. A. Orszag, *Numerical analysis of spectral methods: theory and applications*, CBMS-NSF Regional Conference Series in Applied Math, SIAM (1983)

10. H. E. Huppert and D.R. Moore, J. Fluid Mech. 78, 821 (1976)

11. G. Iooss and D. D. Joseph, *Elementary stability and bifurcation theory*, Springer Verlag New York (1980)

12. D. D. Joseph and Y. Y. Renardy, *Fundamentals of Two-Fluid Dynamics*, Springer Verlag New York (1993)

13. E. Knobloch, in *Proceedings of the 1985 Joint ASCE-ASME Mechanics Conference*, ed. N. E. Bixler and E. A. Spiegel, Vol. 17, Fluid Eng. Div., ASME, New York (1985)

14. E. Knobloch, A. E. Deane, J. Toomre, and D. R. Moore, Contemp. Math. 56, 203 (1986)

15. W. Nagata and J. Thomas, SIAM J. Math. Anal. 17, 91 (1984)

16. W. Nagata and J. Thomas, SIAM J. Math. Anal. 17, 289 (1984)

17. S. A. Orszag, J. Fluid Mech. 50, 689 (1971)

18. M. R. E. Proctor and J. Y. Holyer, J. Fluid Mech. 168, 241 (1986)

19. M. Renardy and Y. Renardy, Physica D 32, 227 (1988)

20. M. Renardy and Y. Renardy, ZAMP 43, 154 (1992)

21. Y. Y. Renardy, Phys. Fluids A 5, 1376 (1993)

22. M. Roberts, J. W. Swift and D. H. Wagner, Contemp. Math. 56, 283 (1986)

23. D. Ruelle, Arch. Rat. Mech. Anal. 51, 136 (1973)

24. R. W. Schmitt, Ann. Rev. Fluid Mech. 26, 255 (1994 a)

25. R. W. Schmitt, J. Phys. Ocean. 24, (4) 855 (1994 b)

26. R. W. Schmitt, J. Phys. Ocean. 25, (1) (1995)

27. M. Silber and E. Knobloch, Nonlinearity 4, 1063 (1991)

28. M. Silber, H. Riecke and L. Kramer, Physica D 61, 260 (1992)

29. M. E. Stern, Tellus 12, 172 (1960)

30. H. Stommel, A. B. Aarons and D. Blanchard, Deep-Sea Res. 3, 152.

31. J. W. Swift, Nonlinearity 1, 333 (1988)

J. 32S. Turner, *Buoyancy Effects in Fluids*, Cambridge University Press (1979)

33. J. S. Turner and H. Stommel, Proc. Natl. Acad. Sci. 52, 49 (1964)